Laser-pyrolysis and flammability testing of graphite flame-retarded polyethylene

by

Cebolenkosi Mbonane

A dissertation submitted in partial fulfilment
of the requirements for the degree

Master of Science Applied Science (Chemical Technology)

in the

Department of Chemical Engineering
Faculty of Engineering, the Built Environment and Information Technology

University of Pretoria
Pretoria

February 2018

DECLARATION

I, Cebolenkosi Mbonane, Student No. 12241602, do hereby declare that this research is my own original work and that to the best of my knowledge and belief, it has not been previously submitted in its entirety or in part and is not currently being submitted either in whole or in part at any university for a degree or diploma, and that all references are acknowledged.

SIGNED on this 6th day of February 2018

_____

Cebolenkosi Mbonane

Laser-pyrolysis and flammability testing of graphite flame-retarded polyethylene

Cebolenkosi Mbonane

ABSTRACT

The fire behaviour of linear low-density polyethylene composites containing 10 wt.% of different carbon-based fillers was studied. Cone calorimeter tests conducted at a heat flux of 35 $kW \cdot m^{-2}$ showed that the expandable graphite sample reduced the peak heat release rate by about 50 % while the flake graphite increased the ignition time by about 80 %. Pyrolysis combustion flow calorimetry results were practically identical for all composites. This reveals shortcomings of this bench-scale flammability test method when the flame retardancy mechanisms relies on either the development of physical barrier layer at the surface of the burning sample or on reflecting the incident heat flux. Similarly, it was found that laser pyrolysis-thermogravimetric analysis generated outcomes that did not correlate with the cone calorimeter results at all. In particular, the composite based on expandable graphite performed poorly. The likely explanation is that the aspect ratios of the small samples were such that the barrier effects on which this system relies, was negated by edge effects.

Keywords: Flame retardant; polyethylene; graphite; laser pyrolysis

ACKNOWLEDGEMENTS

I would like to express my sincere gratitude to:

- Prof Walter W Focke and Dr Bonex Wakufwa Mwakikunga for the encouragement, guidance, support and all contributions throughout the study.
- The CSIR National Laser Centre, CSIR Nano-Structured Materials, Southern Education Research Alliance (SERA), Institute of Applied Materials and the SARChI Chair in Carbon Materials and Technology of the University of Pretoria (UP).
- All of my fellow researchers at the Institute of Applied Materials (UP) which include: Washington Mhike, Mthokozisi Sibanda and Shepherd Tichapondwa for all the support and invaluable suggestions.
- All of my fellow researchers at the CSIR Nano-Structured Materials for all the support and hospitality.
- My family, parents Dudu and Muntu, and Uncle Msawenkosi Khanyile and Malusi Ngema for their support, encouragement and compassion.
- My daughter Ukukhanya for nurturing the breaths I take.
- The universe for the openness it has shown towards the nature of our beliefs, religions, hypotheses and theories. Invariantly providing freedom which is ought to be found when proclaimed or searched and carefully embedded or proved, mirroring exclusive desires or the truth. Thus I embrace humanity as one, as we continue to construct and reshape necessities in favour of the envisioned *better life for all*, while we wait for the alluring Heaven and Hell realities.

TABLE OF CONTENTS

LIST OF FIGURES

LIST OF TABLES

ABBREVIATIONS

ASTM	American Society for Testing Materials
BET	Brunauer-Emmett-Teller
CB	Carbon black
CC	Cone calorimeter
CDGC	Carbon dioxide generation calorimeter
EG	Expandable graphite
ES 250 B5	Low temperature Expandable graphite and exfoliated (expanded) graphite
ES 170 300A	Expandable graphite
FIGRA	Fire growth rate
FTICR	Fourier transform ion cyclotron resonance
FTIR	Fourier transform infrared
HRR	Heat release rate
ICAL	Intermediate-Scale calorimeter
ITMS	ion trap mass spectroscopy
LLDPE	linear low density polyethylene
LPy	Laser pyrolysis
ISO	International standards organization
MARHE	Maximum average rate of heat emission
NASA	National Aeronautics and Space Administration
NBS	National bureau of standards
NFPA	National Fire Protection Association
NIST	National Institute of Standards and Technology
OCGC	Oxygen consumption generation calorimeter
OC	Oxygen consumption calorimeter
PAHs	Polycyclic aromatic hydrocarbons
PE	polyethylene
PCFC	Pyrolysis combustion flow calorimeter
PGC	Pyrolysis gas chromatography
pHRR	peak heat release rate
QMS	Quadrupole mass spectroscopy
SERS	Surface-enhanced Raman scattering

TGA	Thermogravimetric analyser
ToFMS	Time-of-flight mass spectroscopy
wt.%	Weight percent
XRD	X-ray diffraction
XRF	X-ray fluorescence
ZG	Zimbabwe graphite

NOMENCLATURE

Symbol	Description	Units
$\boldsymbol{A_c}$	Frequency factor for char formation	s^{-1}
$\boldsymbol{A_g}$	Frequency factor for gaseous volatiles formation	s^{-1}
$\boldsymbol{c}$	Material specific capacity	$J{\cdot}K^{-1}{\cdot}s^{-2}$
C_p	Specific heat capacity of the gas	$J{\cdot}kg^{-1}{\cdot}K^{-1}$
$d\aleph/dt$	Moles of gas reacting per unit time per unit volume	$mol{\cdot}s^{-1}$
$\boldsymbol{dP'}$	Polymer differential mass	kg^{-1}
$\boldsymbol{dQ}$	Change in heat content	J
$\boldsymbol{dU}$	Change in internal energy	J
$\boldsymbol{dV}$	Change in volume	m^{-3}
$\boldsymbol{E_a}$	Activation energy	$kJ{\cdot}mol^{-1}$
$\boldsymbol{E_c}$	Activation energy for char formation	$kJ{\cdot}mol^{-1}$
$\boldsymbol{E_g}$	Activation energy for gaseous volatiles formation	$kJ{\cdot}mol^{-1}$
$\boldsymbol{E_{o_2}}$	Energy coefficient for oxygen consumption: $\mathbf{13.1 \pm 0.7\ MJ\ kg^{-1}}$ of $\boldsymbol{O_2}$	$MJ{\cdot}kg^{-1}$
$\boldsymbol{E_{co_2}}$	Energy coefficient for carbon dioxide generated: $\mathbf{13.3 \pm 1.5\ MJ\ kg^{-1}}$ of $\boldsymbol{CO_2}$	$MJ{\cdot}kg^{-1}$
$\boldsymbol{E_{o_2(co\rightarrow co_2)}}$	Energy coefficient for oxygen consumption during the generation of $\boldsymbol{CO_2}$ from $\boldsymbol{CO}$	$kJ{\cdot}kg^{-1}$
$\boldsymbol{HRC}$	Heat release capacity	$MJ{\cdot}kg^{-1}{\cdot}K^{-1}$
$\boldsymbol{HRR}$	Heat release rate	$kW{\cdot}kg^{-1}$
$\boldsymbol{k_c}$	Rate constant for char generation in Arrhenius form	s^{-1}
$\boldsymbol{k_g}$	Rate constant for gaseous volatiles generation in Arrhenius form	s^{-1}
$\boldsymbol{k_p}$	Rate constant which is the difference in initiation process and recombination process during polymer degradation	$mol{\cdot}s^{-1}$
$\boldsymbol{m_i}$	Mass of the i^{th} component	kg
$\boldsymbol{m}$	Mass of sample material	kg
M_i	Molar mass of the i^{th} component	$kg{\cdot}mol^{-1}$
$\boldsymbol{m(T)}$	Mass as a function of temperature	kg
$\boldsymbol{m'}$	Mass fraction of the residue mass	kg

$\dot{m}_{o_2}^0$	Mass flow rate of O_2 through the exhaust duct when there is no combustion	kg·s^{-1}
$\dot{m}_{co_2}^0$	Mass flow rate of CO_2 through the exhaust duct when there is no combustion	kg·s^{-1}
$\dot{m}_{o_2(co\rightarrow co_2)}$	Mass flow rate of oxygen which combusted CO to produce CO_2	kg·s^{-1}
P	Pressure	Pa
P_0	Initial mass of polymer	kg
p_i	Partial pressure of the i^{th} species	Pa or N·m^{-2}
$\dot{Q}_{OC}$	Heat release rate (HRR) by oxygen consumption calorimetry	kW·kg^{-1}
$\dot{Q}_{CDG}$	Heat release rate (HRR) by carbon dioxide generation calorimetry	kW·kg^{-1}
$\dot{Q}$	Time derivative of the change in heat content	W
$\widetilde{Q}^V$	Energy density generated in the gas phase for the well mixed fuel-air mixture reaction	J·m^{-3}
R	Arrhenius Gas constant	s^{-1}
S	Surface area	m^{-2}
t_{ign}	Time to ignition	s
T	Temperature	°C
T_a	Ambient temperature	°C
T_p	Temperature of maximum mass loss rate	K
x	Distance of the evolved volatile volume element from the window	m

Greek letters

α_i	Absorption coefficient of the i^{th} species	m^2·mol^{-1}
β	Temperature scan rate	K·s^{-1}
ε	Emissivity	-
κ	Thermal conductivity	W·m^{-1}·K^{-1}
γ	Rate constant for temperature rise. Depends on the laser beam energy, absorbance and emissivity of the composite	s^{-1}
ρ	Sample material density	kg·m^{-3}
α	Thermal diffusivity	m^2·s^{-1}
σ	Stefan-Boltzmann constant	W·m^{-2}·K^{-4}

Φ_{ex}	Transmitted light beam	$W \cdot m^{-2}$
ΔH_c	Heat of combustion of the fuel gases per unit initial mass of solid	$MJ \cdot kg^{-1}$
ΔV	Volume element of the precursor aerosol	m^3
$\Delta V/V$	Bulk expansivity of the sample material	-
$\aleph/V$	M.olar density in the volume element	$mol \cdot m^{-3}$
ΔA	Cross-sectional area of the aerosol	m^2
ΔH	Heat of reaction in joule/mole	$J \cdot mol^{-1}$
Δx	Thickness of the volume element	m
$\Delta \dot{\boldsymbol{m}}_{\boldsymbol{o_2}}$	Mass flow rate of $\boldsymbol{O_2}$ consumed	$kg \cdot s^{-1}$
$\Delta \dot{\boldsymbol{m}}_{\boldsymbol{co_2}}$	Mass flow rate of $\boldsymbol{CO_2}$ generated	$kg \cdot s^{-1}$
μ	Inert burn residue fraction	-

CHAPTER 1: INTRODUCTION

1.1 Background

Pyrolysis is a word derived from Greek with *pyro* meaning 'fire' and *lysis* meaning 'separating'. Pyrolysis is the thermochemical decomposition of carbon-based materials in the absence of oxygen. In fire situations it is a first step towards gasification and combustion. This means pyrolysis is different from combustion as the latter requires the presence of oxygen.

Laser processing involves complex photothermal and photochemical processes. A good understanding requires detailed information on the interactions between the laser light and the substrate material. 'Photochemical" refers to the laser-induced process which proceeds non-thermally. If a system involves both photothermal and photochemical mechanisms, the process is called photophysical. Laser pyrolysis leads to fast temperature rises. This leads to unique degradation conditions that may reproduce the conditions in real fire scenarios (Fanter et al., 1972). The pyrolysis behaviour of a material can be effectively analysed with a laser as it can be focussed on a small area and it also provides a distinctive detection sensitivity. Hence, localized heating introduces various advantages such as elimination of secondary reactions which may otherwise occur due to the hot surfaces of the sample cell (Bart, 2005).

However, laser pyrolysis is highly dependent on the optical properties of the sample material. It may be necessary to 'laser sensitize' materials with additives to allow for optimal absorption of the laser beam energy (Bart, 2005). This is because a laser provides monochromatic radiation that may excite only certain bonds in pyrolysing materials. Therefore, efficient laser light absorption may necessitate converting the sample material into an absorbing derivative. For instance, carbon black powder and graphite fillers can be incorporated into polyethylene to facilitate laser beam energy absorption (Focke et al., 2014, Mhike and Focke, 2013, Mhike et al., 2017). However, it has been argued that reinforcing a material with graphite can interfere with the degradation processes and result in reactive radicals at higher laser beam energies (Schaeffer and Pearson, 1969).

Mass spectroscopy (MS) devices such as (quadrupole)Q-MS, (ion trap)IT-MS, (time-of-flight)ToF-MS, Fourier transform ion cyclotron resonance (FTICR-MS) etc., coupled with laser pyrolysis, have been used to track the evolution of volatiles (Bart, 2005).

Standardized fire test (ASTM, 1999, International, 2013, Standard, 2002) methods developed by ASTM, NFPA and ISO, etc. do not employ laser processing in fire testing. These standards include fire tests methods for large (Room Corner Test, ISO 9705, ASTM E 603 and

EN 14390), moderate (Intermediate-Scale Calorimeter (ICAL), ASTM E 1623) and bench scale (or small scale) (Cone Calorimeter, ASTM E 1354, NFPA 271 and ISO 5660) testing.

Large scale fire tests demonstrate the effectiveness of a flame retardant with respect to decreasing the flame spread rate and burning rate of a material (Babrauskas, 1983, Peacock and Babrauskas, 1991). However, the convenience of large scale fire tests is off-set by reproducibility issues and the considerable expense they pose. The development of laboratory-scale fire tests started during the 1950s (Babrauskas, November 2008, Babrauskas, 1984a). Several decades passed before a practical way of measuring the heat release rate (*HRR*) was implemented. In the late 1970s bench-scale fire engineering devices materialized (Babrauskas, 1984b, Babrauskas, 1984a). These tests were based on complex principles and required costly installations. Then, during the early 1980s, the principle of oxygen consumption calorimetry was established. It is based on the fact that that combustion of organic fuels results in a net heat release of 13.1 ± 0.7 MJ/kg O_2 consumed (Huggett, 1980). This allowed the determination of the *HRR* fire parameter to an acceptable accuracy (Huggett, 1980).

Eventually, during the 1980s, a bench-scale fire test instrument, namely the cone calorimeter, was developed at the NBS. It adopted the principle of oxygen consumption calorimetry. This system could measure heat release rate to a reasonable accuracy, and in addition, other vital fire hazard parameters (Babrauskas, 1984b, Babrauskas, 2016a). The rapid mass calorimeter (ISO, 2015) allows for up to 96% savings of material compared to the cone calorimeter with similar results especially with HRR characteristics (Rabe and Schartel, 2017). The bench scale tests (Walters and Lyon, 1997) brought almost limitless advantages, from reducing costs to enabling a finer investigation of material fire-behaviour parameters, which in the past could not be efficiently established on a larger scale (Babrauskas, 1984a, Babrauskas and Peacock, 1992, Janssens and Parker, 1992).

Reducing the rate of mass loss of a composite material leads to a slower evolution of volatiles and it is also expected to lower the *HRR*. This is usually done by incorporating fire retardants in polymeric materials during and/or after synthesis. Conventional flame retardants can increase the time to ignition and reduce the rate of fire spread but they may increase the potency of the toxic gases that are released. The *HRR* is considered to be single most important parameter in fire hazard assessment (Lyon, 2000a, Babrauskas and Peacock, 1992).

The shortcomings of bench-scale testing is that larger polymer sheets in large-scale fire test may be pose significantly different fire hazard issues compared to smaller test sheets which are subject to weaker ignition sources. However, one should acknowledge that appropriate

experimental and mathematical models have been developed to bridge this gap (Babrauskas, 1991, Babrauskas, January 1991, Babrauskas, November 2008).

1.2 Aims and Objectives

This study explored the idea of a laser-based flammability tester for testing the fire behaviour of small materials samples. As a first step, the fire behaviour of polyethylene composites were investigated and the results compared to the outcomes of laser pyrolysis-thermogravimetric analysis (LPy-TGA) experiments. The polyethylene samples were reinforced with different forms of graphite. The fire behaviour of the composites was evaluated in cone calorimeter tests as well as in a pyrolysis combustion flow calorimeter (PCFC) tests and compare to LPy-TGA results. The purpose was to determine the reproducibility of LPy-TGA results and to establish whether results obtained in the different tests correlate with each other.

1.3 Outline of study

The Dissertation comprises five chapters. The Chapter 1 introduces the subject and this is followed by a literature review presented in Chapter 2. The review covers an outline of the fundamentals of lasers and laser technology. The nature of fire is introduced and the basics are outlined. The flammability of polymeric materials is discussed. Selected fire test methods are reviewed and compared and fire hazard parameters are outlined. The experimental procedures and material characterization methods are discussed in in Chapter 3. The results are presented and discussed in Chapter 4. The final chapter lists pertinent conclusions and it also makes some recommendations.

CHAPTER 2: LITERATURE

2.1 Laser Technology

Laser is an acronym for “Light Amplification by Stimulated Emission of Radiation” and it refers to the physical process necessary for the production of laser radiation. Figure 1 shows a laser active medium or optical resonator (e.g. solid, liquid or gas) that is supplied with energy to excite the atoms, molecules or ion through a process called “pumping”. The source supplying the required energy depends on an active medium. This could be another laser, an applied voltage, flash lamps or even an electrical gas discharge. The energy source excites the atoms leading to the emission of photons. The emitted photons collide with other atoms in the excited state which then also emit photons of the same wavelength, phase and direction as the incident photons. This process is called stimulated emission. Laser radiation is monochromatic, coherent and non-divergent.

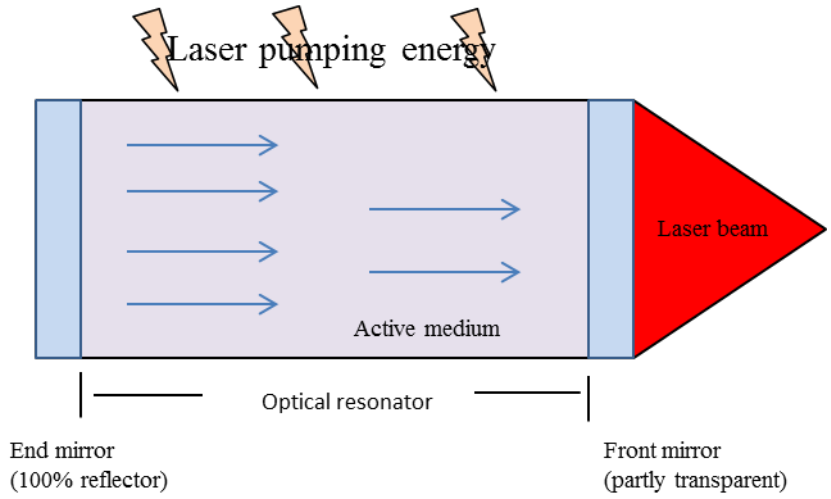

Figure 1: Schematic of a laser resonator structure.

The resonator may be a gas-filled tube or a solid which may be a ruby or a semiconductor with mirrors placed at both ends where the radiation is reflected. Figure 2 show where different lasers fit into the electromagnetic spectrum and Figure 3 illustrates possible laser modes (continuous or pulse laser).

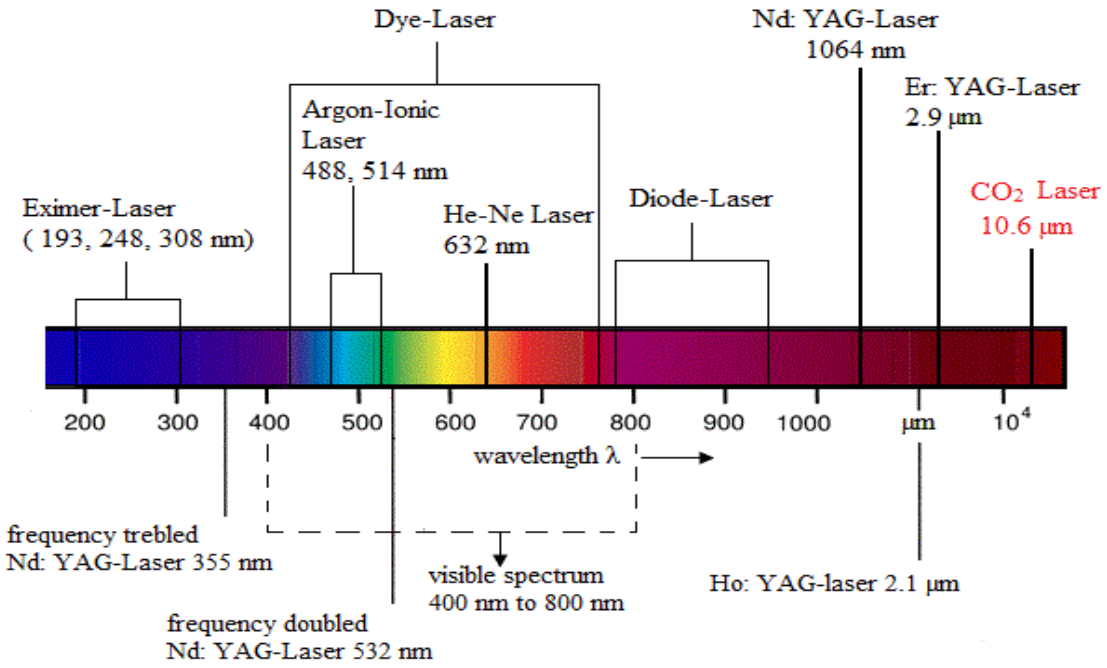

Figure 2: Laser type allocation in the electromagnetic spectrum.

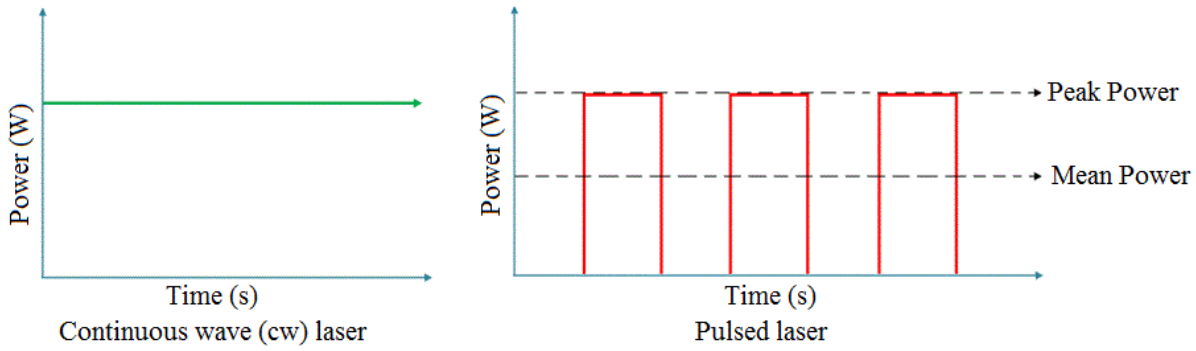

Figure 3: Laser constitute either continuous wave or pulsed beam propagation mode.

2.2 Lasers and polymers

Certain process specifics and material restrictions must be taken to account in order to enable laser processing. The material may have to be “laser sensitized” with the addition of additives to facilitate absorption of the laser radiation. This enables the conversion of laser energy into heat. Since polymers often do not absorb radiation in the wavelength region extending from the near ultraviolet to the near infrared. This means that, without additives, polymers can only be studied in the far infrared with CO_2 lasers and in the far ultraviolet with excimer lasers as seen in Figure 4.

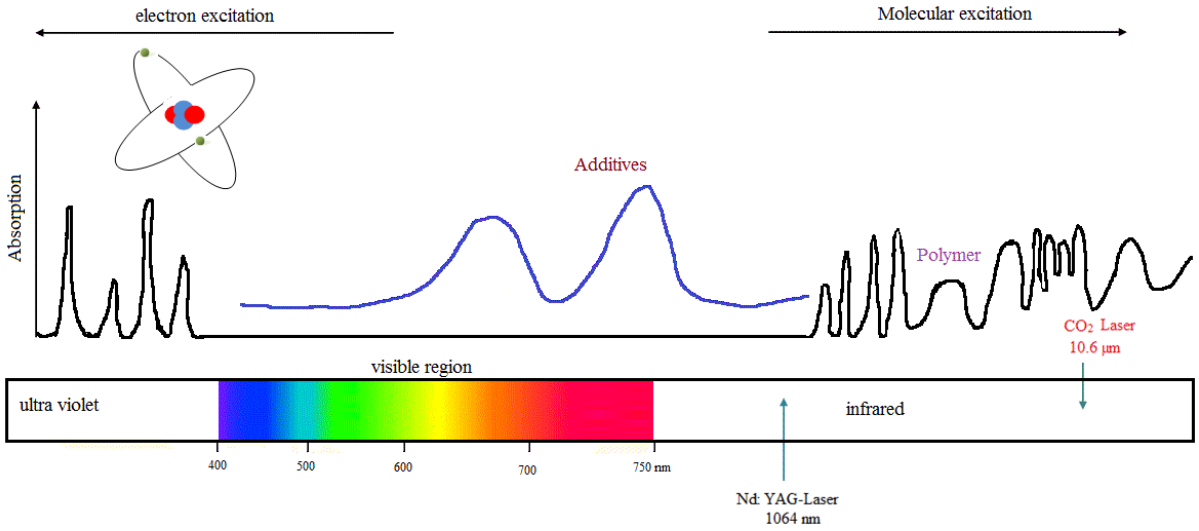

Figure 4: The schematic of Laser light selection between ultra violet and infrared in the electromagnetic spectrum with respect to additives and polymers.

In Figure 5 the incident laser beam strikes an interface between two media (e.g. air and sample material) with different refractive indices. Part of the beam is reflected at the interface and the other part is may be absorbed as it penetrates; the rest of radiation is transmitted. Depending on the surface orientation (smooth or rough surface) different types of reflections can be achieved (specular, diffuse or spread). The material properties are significant during these effects and the sum of all radiations equals 100 %. A fraction of the absorbed light is converted into heat and some is lost through scattering. The reflection and transmission intensities of the polymer are determined by the ratios of the absorption coefficients and refractive indices. Reflection is defined by the angle of incidence α which is equal to the angle of reflection θ of the light beam. Electromagnetic wave scattering may result as a consequence of structural defects in the materials, which could be caused by poor distribution of additives, air pockets, etc.

The transparency of a medium e.g. in electromagnetic waves is measured by transmission, where transmittance defines the quantity of the light flux or incident laser radiation that fully penetrates a transparent component. The transmittance τ is given by

$$\tau = \Phi_{ex} / \Phi_{in} \qquad (2\text{-}1)$$

where Φ_{ex} is the transmitted light beam and Φ_{in} incident beam. Transmittance depends on the wavelength or frequency of the electromagnetic radiation and the angle of incidence of the wave as well as the refractive indices of the materials under consideration.

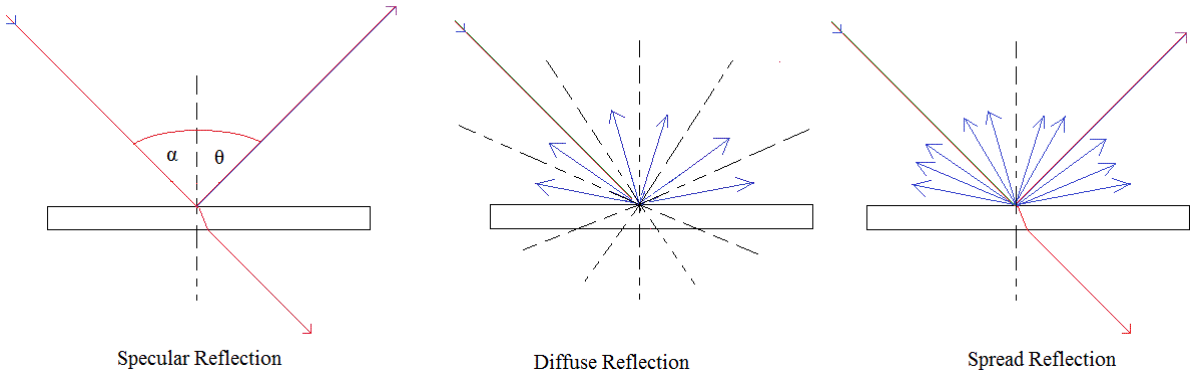

Figure 5: The schematic example of laser light interaction with a polymer. For specular reflection, diffuse reflection, spread reflection. The angle of incidence α is equal to the angle of reflection θ in specular reflection. Spread reflection involves both specular and diffuse reflection.

2.3 Laser pyrolysis

The continuous wave CO_2 laser in this study was coupled to an in-situ thermogravimetric analyser (TGA) to enable photo-thermal and photo-chemical processes analysis on materials. The energy-balance equation based for laser-pyrolysis was previously established (Haggerty and Cannon, 1981). The equation can be applied to explain LPy-TGA. The energy-balance equation states that the energy absorbed by a sample material from the laser beam is equal to the sum of the energy used to raise the sample material temperature, to induce chemical reactions, and to account for the losses due to heat transfer which includes radiation, conduction and convection. The energy losses were incorporated in Haggerty and Cannon energy balance equation by (Mwakikunga et al., 2008) in 2011. The equation is given here as:

$$I_0 \Delta A e^{-\sum \alpha_i p_i x}\left[1-e^{-\sum \alpha_i p_i \Delta x}\right] = C_p \frac{\aleph}{V}\Delta V \frac{dT}{dt} + \Delta H \Delta V \frac{d\aleph}{dt} + \varepsilon\sigma A\left(T^4 - T_s^4\right) + \kappa_{conv}\left(T - T_s\right) + K_s 2\pi r_{beam} h\left(T_{\max} - T_{pan}\right) + K_{pan} 2\pi r_{pan} h\left(T_{pan} - T\right) \quad (2.2)$$

where I_0 denotes the input laser intensity in W cm^{-2}, the volume element ΔV, the cross-sectional area ΔA as seen by the laser beam, the absorption coefficient α_i of the i^{th} species, the

partial pressure p_i of the i^{th} species, the distance x of the volume element from the window, the thickness Δx of the volume element, the heat capacity C_p of the material, the molar density $\aleph/V$ in the volume element, the rate of change dT/dt of temperature, the heat of reaction ΔH in joule/mole and the moles of gaseous products evolved during degradation of material reacting per unit time per unit volume, $d\aleph/dt$.

The equation can be modified specifically for LPy-TGA where mass is not constant with time. Then, $\aleph_i$ can be rewritten as $\aleph_i = m_i/M_i$ where m_i and M_i are mass and molar mass of the i^{th} component of a material in the composite sample under investigation. The time changing temperature T can be replaced with an expression $T = T_{max}(1\text{-}\exp(-\gamma t))$, where T_{max} is the maximum temperature the sample attains, and γ is the factor that will depend on the laser beam energy, absorbance and emissivity of the composite. Therefore equation (2.3.1) can be written as:

$$I_0 \Delta A e^{-\sum \alpha_i p_i x}\left[1-e^{-\sum \alpha_i p_i \Delta x}\right] = \frac{m_i C_p \Delta V}{M_i V} T_{\max} \gamma e^{-\gamma t} + \frac{\Delta H \Delta V}{M_i}\frac{dm_i}{dt} + \varepsilon \sigma A\left[T_{\max}^4\left(1-e^{-\gamma t}\right)^4 - T_s^4\right] + \kappa_{conv}\left(T_{\max}\left(1-e^{-\gamma t}\right)-T_s\right) + 2\pi r_{beam} h K_s\left(T_{\max}-T_{pan}\right) + 2\pi \tau_{pan} h K_{pan}\left(T_{pan}-T\right) \tag{2.3}$$

The parameter $\Delta V/V$ can be referred to as the bulk expansivity of the sample material. The expression describing the variation of sample mass with time and temperature and hence laser beam energy, can be acquired from the solution of the differential equation for mass of i^{th} component, m_i, of the composite, Σm_i, see Appendix I. Such that,

$$m = \sum_{i=1}^{n} m_i \tag{2.4}$$

where Σm_i is the amount of mass lost due to interaction with laser beam, and m_0-Σm_i is the mass that remains in the TGA pan which is referred to as the residual mass., where m_0 is the initial mass of the materials,

The residual mass written as a percentage is given as

$$m_{res}(t,T) = 100\left(1-\frac{m}{m_0}\right) \tag{2.5}$$

CO_2 laser beam wavelength is in the IR range so its effect on a sample material simulates real fire scenario. The laser offers intense beam energy upon a pyrolysis sample resulting in rapid decomposition of material composites. The temperature rise time is predicted

to microseconds, and during pyrolysis explosion-like behaviour of decomposition products result into a 'plume' with temperatures ranging at 500°C to 2000°C (Bart, 2006). This extensive degradation produces species which are characteristic, nonetheless, unique to those found in conventional pyrolysis. The absorption of the laser beam depends on an opacity degree of a material. It is expedient to use laser pyrolysis on 'laser sensitized' materials for maximum absorption of the beam. We will show how Equation 2.3 is employed in the fitting to some of the laser-TGA data from polymeric fire-retarding materials and the extraction of the relevant parameters. This is given the Results section of this dissertation.

Laser degradation of carbon black- and graphite-filled polymer composites leads to the production of a variety of volatile products (Schaeffer and Pearson, 1969). Highly reactive species have been observed with pure graphite (Fanter et al., 1972, Ristau and Vanderborgh, 1971). A LPy-FTIR study (Goldberg et al., 2001) has shown that, at high laser beam energies, the evolved gaseous products can be hardly followed even at the fastest FTIR scanning rates because of the even faster degradation rates induced by the highly reactive radicals present. LPy-GC (pyrolysis gas chromatography) degradation of polyethylene was studied (Fanter et al., 1972). The LPy-GC approach was applied on thin polymeric films placed on a blue plasma glass rod. The plasma glass facilitated the absorption of the laser beam and the GC separated the pyrolysis products that were evolved. The pyrolysis products included ethylene, acetylene, methane, pentene, hexene, benzene and octane. There were variations in the relative amounts with the increase in laser energy with more stable compounds forming at higher temperatures. Reproducible results were obtained with transparent materials subjected to laser pyrolysis coupled with surface-enhanced Raman scattering (SERS) (Zhou et al., 2003). LPy-TGA provided an advantage for studying the temperature changes during pyrolysis and the rate of change in mass. The mass loss rate is understood to provide a good indication of the rate of heat released by a material. In fact, there is a strong correlation between mass loss rate and heat release rate (Thornton, 1917, Mouritza, 2005).

Thermogravimetric analysis with CO_2 laser heating has been reported (Anon, 2001). The Thiokol Corporation developed the technique in order to obtain time-resolved data on the thermal decomposition of specimens of a solid material that are exposed to a heat flux comparable to the heat flux in a typical rocket engine. In the experimental setup the specimens were heated with continuous-wave laser beams to obtain the required high heat flux. The laser TGA could be used to study high-heating-rate thermal decomposition of almost any high-temperature insulating material.

2.4 Fire behaviour of polymers

A polymer is a molecule made of repeating chemical units called monomers. There are three main classes of polymers: thermoplastics, thermosets and elastomers. Thermoplastics do not change chemically on heating but can repeatedly be melted and shaped. Thermosets are polymers that undergo chemical changes causing them to permanently solidify during curing through crosslinking reactions. Once the part is made it cannot be re-shaped by simple heating. Elastomers can either be thermoplastics or thermosets but they are distinguished by a unique elasticity, usually associated with a low Young's modulus and a high failure strain.

The organic nature of a polymer is defined by a chemical structure comprising mainly carbon and hydrogen, and often oxygen too. The combustible nature of polymers derives from the hydrocarbon nature dominated by carbon-carbon and carbon-hydrogen bonds. Polymers burn as a result of thermal degradation that releases combustible decomposition products (Fanter et al., 1972). Elevated temperatures, induced by an external heat source, induce chemical bond scission with the consequence that volatiles are released that diffuse into air (Beyler and Hirschler, 2002). The gaseous volatiles present a fuel that can ignite and result in a flame.

There are natural (DNA, proteins, rubber etc.) and synthetic organic polymers (polyethylene, nylon). Commodity polymers are large volume inexpensive commercial plastics (polyethylene, polypropylene, polystyrene etc.) and they represent about 95% of the total in use (Hull and Kandola, 2009). Unmodified commodity polymers are usually highly flammable which increases the fire risk in homes and commercial areas (Tewarson and Pion, 1976).

Fluoropolymers and engineering polymers with aromatic backbones have a higher thermal stability allowing them to resist ignition and enabling them to self-extinguish (Hull and Kandola, 2009). Polymer fire resistance strongly correlates with its heat release capacity. Fluoropolymers feature a lower heat release capacity (Gandhi et al., 1999, Walters et al., 2000).

2.4.1 Combustion processes

Combustion is “a chemical process of oxidation that occurs at a rate fast enough to produce temperature rise and usually light, either as a glow or flame” (Carpenter et al., 2005). There are physical and chemical aspects of the combustion process (Di Blasi, 1993). The physical combustion aspect affects the oxidation in the solid phase, particularly smouldering combustion (Ohlemiller, 1986, Rein, 2009). The chemical aspects of combustion process relate in particular to the gas phase oxidation, i.e. flaming combustion (Lyon, 2000b, Ohlemiller, 1986, Shafizadeh, 1984).

Consider a polymeric material or product acted upon by a heat source that imparts thermal energy. Initially, the heat energy destabilises the material state (Beyler and Hirschler, 2002) leading to phase changes such as melting, or transformations such as swelling, flowing and deformation (Walters et al., 2000). Thermal degradation is an endothermic process that through bond-breaking results in the evolution of volatile products of low-molecular-weight. The accumulation of volatile species mixed with air generates conditions favourable for combustion. This may lead to smouldering or flaming combustion if the conditions are favourable. There are complex elementary chemical reactions involved in the combustion of a solid fuel. However, the global result of the combustion process can be estimated by two intertwined chemical pathways, i.e. pyrolysis following oxidation (Rein, 2009):

Pyrolysis: The initial step responsible for endothermic chemical decomposition

$$\text{Fuel (solid)} + \text{Heat} \rightarrow \text{Pyrolyzate (gas)} + \text{Char (solid)} + \text{Ash (solid)} \quad \text{(a)}$$

Heterogeneous oxidation: Characteristic for smouldering combustion

$$\text{Char (solid)} + O_2\,\text{(gas)} \rightarrow \text{Heat} + CO_2 + H_2O + \text{other gases} + \text{Ash (solid)} \quad \text{(b)}$$

Gas-phase oxidation: Characteristic for flaming combustion

$$\text{Pyrolyzate (gas)} + O_2\,\text{(gas)} \rightarrow \text{Heat} + CO_2 + H_2O + \text{other gases} \quad \text{(c)}$$

The net result of (a) and (b) is the direct oxidation of the fuel:

$$\text{Fuel (solid)} + O_2 \rightarrow \text{Heat} + CO_2 + H_2O + \text{other gases} + \text{Char (solid)} + \text{Ash (solid)} \quad \text{(d)}$$

Flaming Combustion (Figure 6). The pyrolysis products (pyrolyzate) undergo gas phase oxidation resulting in flaming combustion (BERGER and RERO, 2006, Tewarson, 1994). Flaming occurs when the pyrolysis gases are present in sufficient quantities to support ignition (Lyon, 2000b), that is, the fire triangle requirements are fulfilled (Madrzykowski and Stroup, 2008b). The flaming combustion process is self-sustaining if burning pyrolysis gases supply enough thermal energy back to the material surface resulting in the generation of more flammable volatile products (Cullis and Hirschler, 1981). This process is known as the flame-feedback loop, which enforces the sustained production of reactive volatiles.

Figure 6: Self-sustaining flame in a wood fire during flaming combustion.

Figure 7: Smouldering combustion, a result of char oxidation, smouldering embers and ash residue (Nielsen, 2017)

Smouldering Combustion (Figure 7). Smouldering is a low temperature, slow and flameless burning of condensed porous fuel and is known to be the most persistent combustion phenomena (Rein, 2009, Hurley et al., 2015). Smouldering combustion is a result of a heterogeneous reaction between the solid fuel and the gaseous oxidant species. Typically it is the oxidation of the solid char residue that remains after pyrolysis. Char is a carbon-rich, porous material with high heat of reaction and a large surface-to-volume ratio which can form ash on oxidation. Ash is the mineral-rich residue of a fire with negligible reactivity. Smouldering is exemplified by the burning of charcoal or wood once the visible flames die off. A smouldering fire can also arise in the absence of any external heat source. It can result from the self-heated fuel-initiated ignition inside large heaps of piled fuels (e.g. coal fines) (Ohlemiller, 1985, Ohlemiller, 1986). This is a well know issue in process industries which store large quantities of carbon-rich materials (organic powders, waste, etc.) and it even leads to residential fires (Rein, 2009). Smouldering temperatures typically range from 400°C to 700°C. However, in dense and energetic fuels like coal the temperature can reach about 1000°C.

2.4.2 The burning process

Flaming combustion is the result of physical and chemical processes which occur in three different phases, that is, the gas, the mesophase and the condensed phase (Tewarson, 2002a). The mesophase is the interface region between the gas phase and condensed phase. The energy transport between the gas phase and the mesophase occurs by radiation and convection. Energy is lost from the mesophase by vaporisation of pyrolysis products and in the condensed phase by conduction. Figure 8 shows a model for the burning of a solid polymer material. The

mesophase polymer decomposes during the burning process resulting in charring and the evolution of the pyrolysis gases. The latter are crucial for flaming combustion in the gas phase. The energy balance equations leading to flaming combustion is explored in APPENDIX II: Combustion gas phase kinetics and APPENDIX III: Energy balance equations for the burning of a polymer.

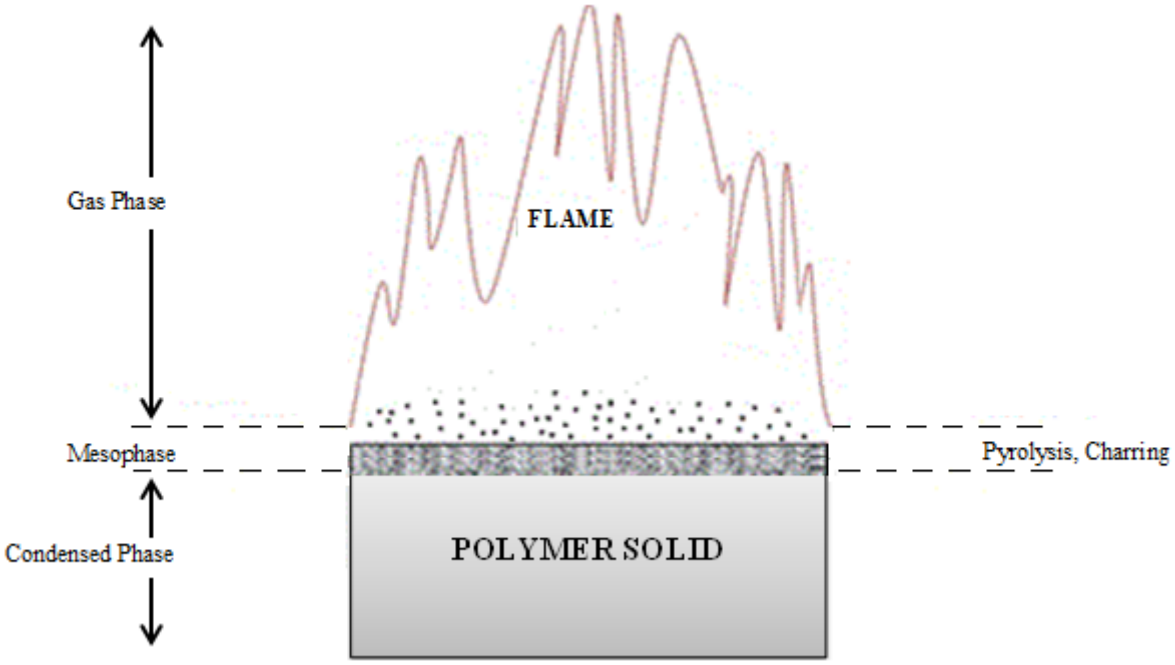

Figure 8: The schematic presents different phases involve during burning of polymer slab (Tewarson, 2002a).

The rate of heat and mass transport are key in flaming combustion. The governing equations describing the heat transfer processes are presented in Appendix III. The material thermally degrades as a result of a physical process, and the volatile pyrolysis products diffuse into air. Consequently, pyrolysis products combust as the fuel and air mixes and this produces radiant energy across the wavelength spectrum. The main pyrolysis products can be represented by a scheme of first order thermal degradation processes which sufficiently represent the kinetics of fuel generation in the mesophase given as (Lyon and Janssens, 2005)

Mesophase. A series of processes define the thermal degradation of a polymer at rate constant k_d leading to a *reactive* intermediate state I*. At this state the gas (G) is produced with rate constant k_g and/or the char (C) with k_c.

$$\text{Polymer} \xrightarrow{k_d} \text{Intermediate}(I^*)$$
$$I^* \xrightarrow{k_g} \text{Gas } (G)$$
$$I^* \xrightarrow{k_c} \text{Char } (C)$$

The burning rate is particularly sensitive to chemical reactions which involve active radicals (see **APPENDIX II: Combustion gas phase kinetics**) from fuel (R), oxygen (O), hydrogen (H), hydroxyl (OH) and phosphorus or halogen (X) (Lyon, 2000a). However, irrespective of the reaction kinetics, sustained flaming often leads to complete combustion. The final products, for complete conversion in the reaction between air (N_2 and O_2) and a generic fuel are carbon dioxide (CO_2), water (H_2O), nitrogen (N_2), and mineral acid (HX). This is summarised by the following reaction scheme (Lyon, 2000a, Walters and Lyon, 2003):

$$C_cH_hO_mN_nX_x + \left(\frac{4c+h-x-2m}{4}\right)O_2 \rightarrow cCO_2 + \frac{h-x}{2}H_2O + \frac{n}{2}N_2 + xHX$$

2.5 Fire risks

Fire is a chemical reaction process which leads to the emission of heat and light at different intensities. The fire triangle refers to three vital elements to start the burning process, i.e. (1) heat flux from a source that drives decomposition of the material and producing (2) fuel gases which lead to ignition if the mass ratio matches the required amount of (3) the oxygen from air (Terrill et al., 1978). The fire can be extinguished by suppressing the availability of one or more of the components of the fire triangle, for example by introducing fire-retardants in the material. The fire tetrahedron refers to the conditions necessary to sustain a flaming fire (DiGuiseppi et al., 1998). These include sufficient fuel vapour or gaseous fuel resulting from an external source or the material's own burning flame providing heat feedback.

A material poses a flammability hazard if there is sufficient fuel vapour to support uninhibited chemical chain reactions (Madrzykowski and Stroup, 2008b). Flammability refers to ignitibility and the rapid burning of a substance. Ignitibility is the ease at which a material yields a self-sustaining, flaming combustion state when exposed to an external heat flux. The fire hazard (BERGER and RERO, 2006) is characterized by the ease of ignition, extreme heat from the flaming material, flame spread (which may lead to nearby materials burning) and the combustion products (EMMONS, 1992, Tewarson, 1994). Difficulties associated with

extinguishing a flaming material also presents a flammability hazard (Hartzell and Emmons, 1988, Madrzykowski and Stroup, 2008b).

During combustion material gaseous products ignite when they reach the auto-ignition temperature. This is the lowest temperature at which the material spontaneously ignites in normal atmosphere even in the absence of an external source of ignition, i.e. a flame or a spark. (Kashiwagi, 1979, Kishore and Sankaralingam, 1986). However, the material may ignite at a lower temperature, the flash point, when exposed to an intense external heat source. This could be simply a spark or another rapidly burning heat source. It has been noted that fire conditions are the intrinsic property of material flammability, e.g. developed fires could destroy anything nearby (BERGER and RERO, 2006). However, material characteristics can play a crucial role in terms of perpetrating or resisting fire. This also means that the physical nature of a material can present significant outcome in resisting ignition. Certain untreated natural material (e.g. paper, cotton etc.) are prone to ignition because they can release volatile pyrolysis products at relatively low temperatures. Flame retardant reinforced materials feature a reduced degradation rate (Schartel and Hull, 2007a) and fire spread. Flame retardants can slow down the evolution of highly reactive volatiles, and reduce the concentration of reactive radicals through chemical reactions in the gas phase, thus reducing degradation rate and fire spread.

2.6 Flame retardants

During thermal decomposition a material can release reactive species which are highly flammable. Flame retardants are additives which are designed to improve the fire-behaviour of a material (Pearce, 2012). They can supress fire physically (Lyon, 1998) or through chemical reactions that reduces the burning rate of a material (Lu and Hamerton, 2002, Pearce, 2012). The flame retardant can also lengthen the time to ignition which is one of the essential parameters determining fire safety.

2.6.1 Physical action

Fire retardants can modify the thermal degradation route followed by the substrate to form a protective barrier layer (solid or gaseous) at or near the interface which decreases the rate of heat (and mass) transfer. This layer may provide a barrier for oxygen keeping it away from the combustibles and thereby reducing the polymer decomposition and fuel generation rates (See **Figure** 9). The flame retardant degradation reaction could be an endothermic reaction. This reduces the substrate temperature below that required for sustained pyrolysis. Decomposition of the flame retardant additive can produce inert gases (e.g. H_2O and CO_2) that dilute the

concentration of fuel species and oxygen in the gas mixture, thereby suppressing ignition. Aluminium trihydrate and magnesium hydroxide operate according to these two mechanisms.

2.6.2 Chemical action

Gas phase reaction -The flame retardant additive can release moieties which react with the highly reactive radical species responsible for gas phase combustion to form inert or less reactive molecules. This reduces the rate of the exothermic reactions and therefore also the rate of heat release. The substrate temperature is decreased as is the rate of pyrolysis and the fire is suppressed.

Solid phase reaction–flame retardants can increase the rate of the bond scissions so that the polymer liquefies rapidly and drips away from the flame. Otherwise the flame retardants may favour a degradation pathway that forms carbonaceous char rather than volatiles. The char may even provide a protective barrier layer against heat transfer and mass transport. Note that these are physical effects that are the consequence of the redirected chemical decomposition pathway. This also reduces the formation of smoke and other combustibles.

Gas-phase active flame retardants. Halogenated flame-retardants are gas phase-active flame retardants (Le Bras, 1998, Lyon, 2007) which suppress the exothermic (oxidation) processes occurring in the flame between oxygen and volatiles (Hilado, 1982, Pal, 1991). They provide halogen radicals in the gas phase that preferentially react with the highly reactive •OH and •H radicals responsible for the oxidation chain reactions. This trapping of the mentioned radicals reduces the rate of combustion, the rate of heat release drops and the systems is cooled down. Less heat is returned to the condensed phase and less flammable volatiles are produced to the point where the system ceases to be a self-sustaining combustion process. See Figure 11.

Intumescent flame retardants. Intumescence refers to the swelling of the material during burning, as it increases in volume and decreases in density as the insulating charred layer is formed. Intumescent flame retardant materials are typically halogen free which makes them more environmentally friendly (“green” product). During thermal degradation they reproduce a carbonaceous char layer (Lyon, 2007, Lyon, 2002) partially limiting the transfer of fuel to gas phase and protecting the underlying material from the heat flux generated by the flames. Charring refers to the physical changes as the material pyrolysis results in a porous carbonaceous residue, usually black in colour. This acts as a protective layer against an external heat source. It suppresses fuel generation from the material below the char layer.

A typical intumescent formulation (See Figure 10) consists of three elements, a latent acid source or a “catalyst” (phosphate or borate derivatives), a carbonization compound or “charring agent” (polyhydroxy compounds, e.g. pentaerythritol) and a blowing agent or “spumific” (e.g., melamine) (Bourbigot, 2004, Bourbigot, 2000). The acid source degrades to form strong mineral acid that dehydrates the carbonific to form the carbon char. The blowing agent decomposes and produces gaseous volatiles which causes the char to swell before setting.

Polymer resistance to fire may also be improved by introducing either inert fillers (e.g. talc or chalk) or active ones which decompose endothermally and evolve inert gases during decomposition (e.g. aluminium trihydrate or magnesium hydroxide). These substances replace combustible mass with non-combustible mass decreasing the amount of fuel available for burning (Le Bras, 1998, Lyon, 2007).

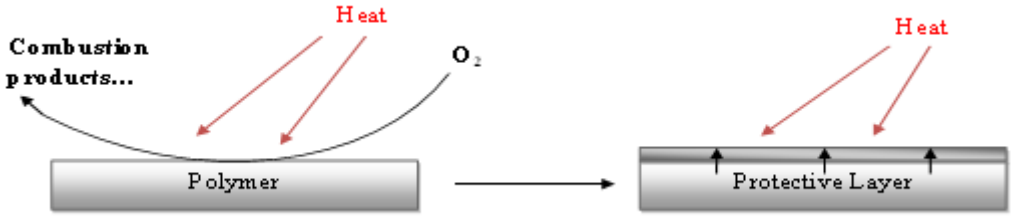

Figure 9: Formation of a protective layer during decomposition of a polymer inhibiting, combustion and volatiles.

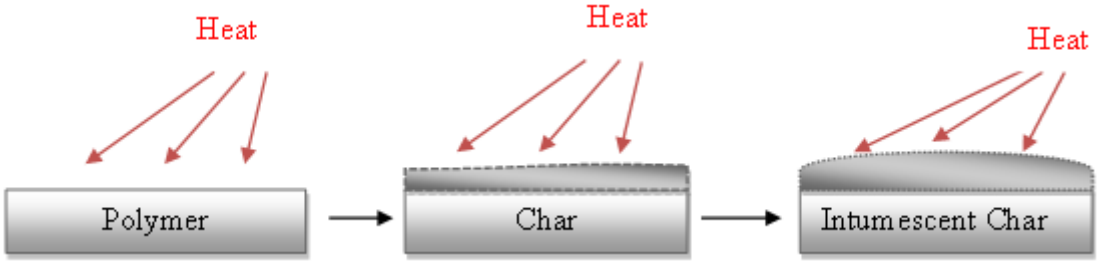

Figure 10: Schematic of a mechanism in char and intumescences’ formation.

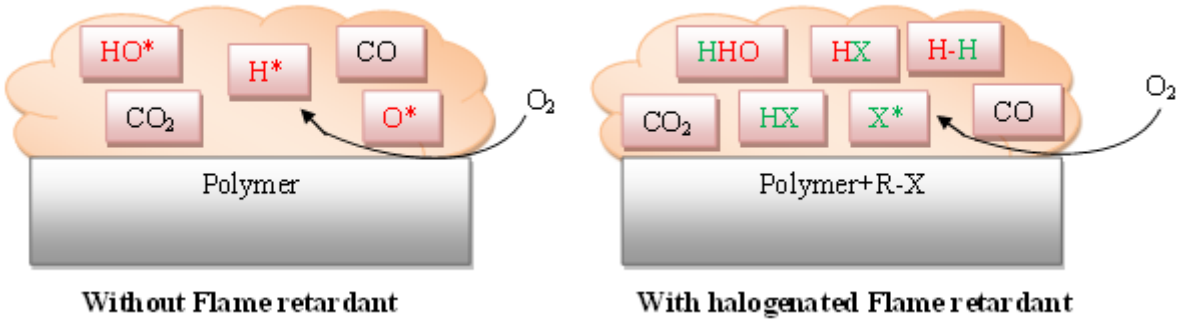

Figure 11: Halogenated flame retardants action mechanism.

2.7 Fire tests

A burning material or product could emit a stream of gaseous volatiles and smoke which could be a hazard to human life and environment. Therefore, product fire tests are necessary to help categorize fire hazard parameter associated with a given product. This is would help develop appropriate improvements and to rank products according to their use, including ways to handle them (CLARKE III and Ottoson, 1975). These products include furniture, garbage bin, toys, mattresses, ceiling board, etc. Large-scale fire tests allow for full scale heat release tests, a necessary property in categorising fire the performance and hazards posed by a product or material (Babrauskas, 1983, Peacock and Babrauskas, 1991). However, such tests can be expensive and complex to conduct (Madrzykowski and Stroup, 2008a). Bench-scale fire test methods have been applied to predict material and product behaviour in full scale fires (Walters et al., 1996, Babrauskas, January 1991). Cone calorimeter test have been used to predict full scale peak heat release rates and products of combustion for furniture products (Babrauskas, November 2008). The heat release rate of a burning material is regarded to be the most important parameter especially in the confined environments with a lack of ventilation (Babrauskas, 2016b, Babrauskas and Peacock, 1992).

2.7.1 Cone Calorimeter

Cone calorimeter (CC) shown in Figure 12 is a widely used fire test method standardized as ASTM E 1354 and ISO 5660-1. Heat release rates of a pyrolysis materials or products can be evaluated using cone calorimetry. This is done by tracking the concentration of pyrolysis gases, oxygen, carbon dioxide and carbon monoxide.

The truncated cone heater represents a 5 kW electrical heating element that generates heat fluxes of up to 100 $kW \cdot m^{-2}$. The radiant heat flux, from electric cone heater, is used to pyrolyse a flat sheet specimen samples typically measuring 100 × 100 × 3.2 mm. The specimen is positioned at about 25 mm below the bottom plate of the cone heater. Ignition is piloted with an electric spark ignitor. The electric spark ignitor is switch off soon as combustion pyrolysis products are ignited. A high-temperature resistant fan extracts the decomposition and/or combustion products through the hood and through the exhaust duct where the composition of the gases is analysed and the smoke obscuration is measured.

The cone calorimeter is also used measure effective heat of combustion, mass loss rate, ignitibility, toxic gases, smoke and soot. The measurement process is based on the oxygen consumption concept (DiNenno, 2008). The cone calorimeter has been used to test a range of

materials (Babrauskas, 1984b, Babrauskas, 2016a). For example, the flammability behaviour of polyethylene reinforced with expandable graphite and intumescent fire-retardant was investigated using the cone calorimeter (Kruger et al., 2014).

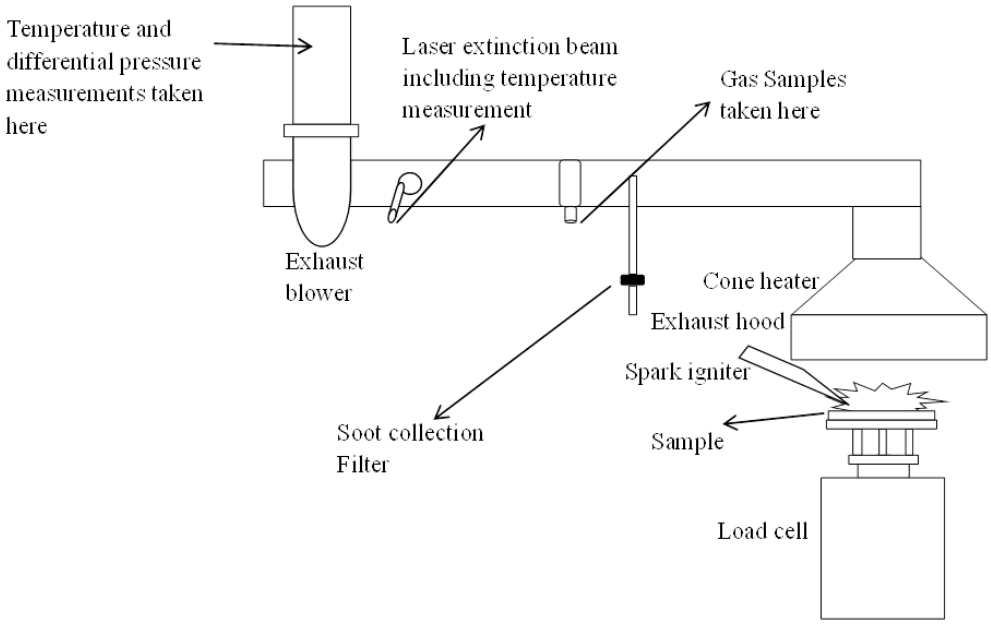

Figure 12: The schematic of the cone calorimeter

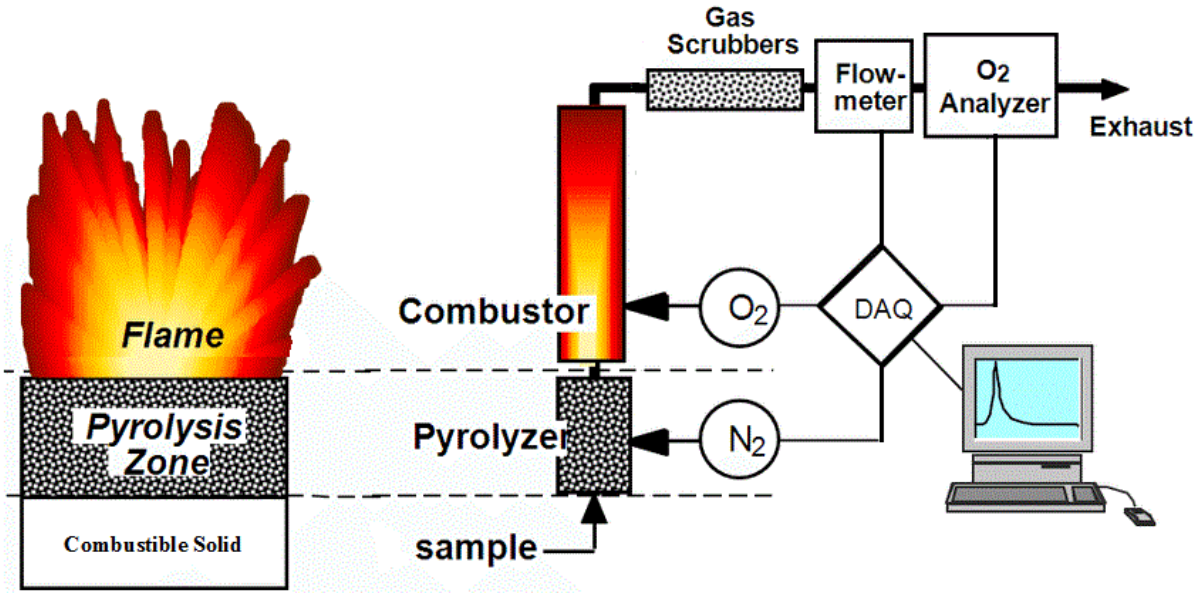

Figure 13: The schematic of the pyrolysis combustion flow calorimeter (PCFC) (Lyon and Walters, 2004).

2.7.2 Pyrolysis combustion flow calorimeter

Pyrolysis combustion flow calorimeter (PCFC) (Figure 13) is a quantitative method for the rate of heat release of combustibles generated by separate pyrolysis of a material. The combustion products are a characteristic that determines the flammability hazard posed by a material. PCFC seeks to reproduce the thermophysical and thermochemical processes under flaming combustion conditions according to a controlled pyrolysis procedure (Lyon and Walters, 2004). The emitted fuel gases are oxidized with excess oxygen under inert atmosphere at high temperatures in a separate chamber. The oxygen consumption calorimetry is used to determine the rate of heat release by the combustion of the gaseous pyrolysis products. PCFC has been coupled with FTIR to analyse combustion products and other flammability hazard properties (Sonnier et al., 2014).

The pyrolysis chamber is in effect a temperature-controlled furnace that is continuously purged with an inert gas (nitrogen). The combustor is simply a coiled combustion tube which is confined in a ceramic furnace able to maintain maximum temperature of 1200°C. The gaseous products emitted are mixed with oxygen (in a ratio so that the final oxygen and nitrogen content reflects the composition of atmospheric air) before they are combusted in second chamber controlled at 900°C (Heffington et al., 1977, Reshetnikov and Reshetnikov, 1999). Gas scrubbers removes other gases from the combustion stream and the oxygen remaining is determined with oxygen analysers. A more detailed explanation of the procedure and illustration of the experimental setup is provided elsewhere (Lyon and Walters, 2004).

2.7.3 Laser pyrolysis-TGA

Figure 14 presents schematically the laser pyrolysis-thermogravimetric analysis (LPy-TGA) setup. It also shows the dimensions of the ceramic crucible that was used. A 632.8 nm HeNe optical laser was used to align the system and pyrolysis was done with a 10.6 nm CO_2 IR laser. This wavelength is in the range of the IR radiation found in real fire scenarios. Polyethylene composites were tested for their pyrolysis behaviour at different isothermal temperatures and laser beam power levels. Prior to laser pyrolysis, sample material was consolidated by heating it to 200°C (i.e. above the melting point of the polymer) and keeping it for 20 min at this isothermal temperature setting in a nitrogen atmosphere. The sample was then left to cool to a pre-set temperature and left there to stabilise for 20 min. Then, with the laser beam properly aligned, laser pyrolysis runs were conducted for another 20 min. TGA was used to follow both the mass loss and the temperature just below the crucible.

2.8 Characterization of Fire Hazard Parameters

Fire hazard has been analysed using different types of calorimeter and computer models. The vital fire development parameters include the heat release rate, the rate and density of smoke generation and the toxic products of combustion (Janssens, November 2008).

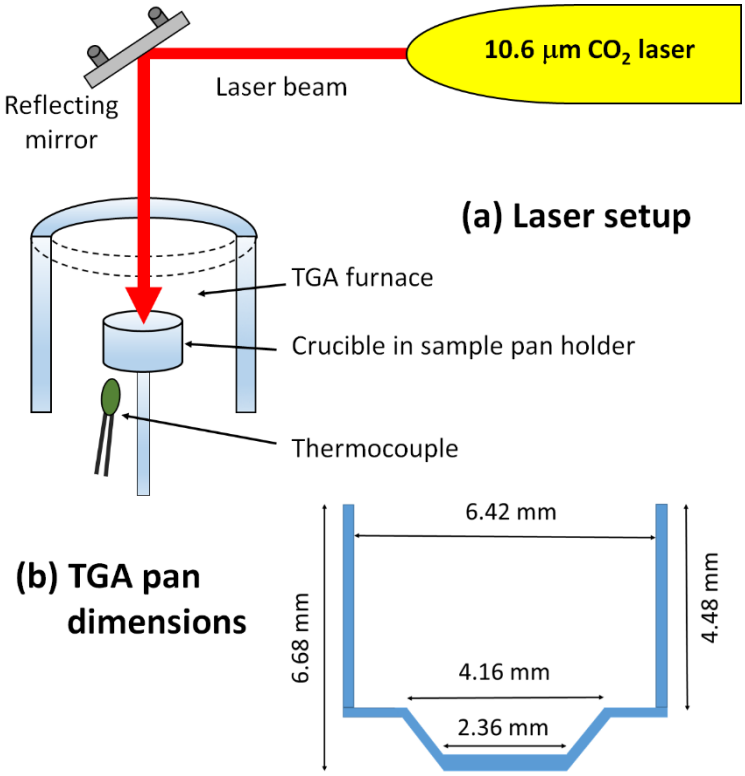

Figure 14: (a) LPy-TGA set-up comprising the power-tuneable CO_2 laser, the TGA chamber comprising the furnace, and a crucible with a thermocouple. **(b)** (Inset) the dimensions of the ceramic crucible.

2.8.1 Heat release rate methods used in Calorimetry

Oxygen consumption (OC) and carbon dioxide generation (CDG) calorimeter. OC is the widely used method for the estimating the *HRR* with high precision and accuracy. The amount of oxygen consumed for complete combustion correlates with the heat released (Thornton, 1917, Mouritza, 2005). Hence, the variations in the concentration of O_2 and absolute heat release per unit mass of O_2 consumed are sufficient to estimate the *HRR* of a complete combustion reaction (Biteau, Sep-2008). The OC principle can be presented as follows:

$$\dot{Q}_{oc} = E_{o_2}\left(\dot{m}^{o}_{o_2} - \dot{m}_{o_2}\right) - \left(E_{o_2(co\rightarrow co_2)} - E_{o_2}\right)\dot{m}_{o_2(co\rightarrow co_2)} \qquad (2.6)$$

The second term is a correction for incomplete combustion which depends on the amount of O_2 needed to oxidize CO to CO_2. For a vast number of organic fuels and solids, E_{o_2} is approximately a constant with an average value of 13.1 MJ·kg^{-1} of O_2 consumed. For standard fuels actual measured values agree to within ± 5% (Huggett, 1980).

The second principle is based on carbon monoxide production and carbon dioxide generation, represented by the following relationship

$$\dot{Q}_{CDG} = E_{co_2}\left(\dot{m}_{co_2} - \dot{m}^{o}_{co_2}\right) + E_{co}\dot{m}_{co} \qquad (2.7)$$

For numerous organic gaseous, liquid and solids compounds the energy released per unit mass of CO_2 generated was constant with an average value of E_{co_2} ca. equals to 13.3 MJ·kg^{-1} of CO_2 produced within ±11% (Tewarson, 2002b). The heat release per unit mass of CO produced was also constant with an average value of E_{co} ca. equals to 11.1 MJ·kg^{-1} of CO produced within ±18%.

2.8.2 Smoke Generation

The International Organization of Standards (ISO) defines smoke as the "visible part of fire effluent". The fire effluent as defined by ISO is the "totality of gases and aerosols, including suspended particles, created by combustion". Smoke and carbon monoxide form part of the fire effluent. ASTM defines smoke as "the airborne solid and liquid particulates and gases evolved when a material undergoes pyrolysis or combustion" (E176-04, 2004). Smoke has also been defined as the component in combustion products that are in the condensed phase (Mulholland, 1995). Smoke includes small particles arising from incomplete combustion. The small particles scatter and absorb light and this causes obscuration. The particles include liquid droplets (resulting from cooling and condensation) (Friedman, 1998) and soot agglomerates which are joined into chains and clusters (Drysdale, 1998, Bond and Bergstrom, 2006). Soot refers to the minute carbon particulates produced in flames that evolving into smoke. During combustion hot soot particulates appear bright as they radiate heat and reflect the yellow glow of the flame. When the soot cools down it becomes dark, and obscures visible light in post-flame smoke. Soot formation and oxidation in flames has been studied over the years (Kennedy, 1997, Beji, 2009, Beji et al., 2011). The assumption is that fuel molecule breakdown results in polycyclic aromatic hydrocarbons (PAHs) which form the basis of soot formation within a flame. The resulting particulate smoke is a product generated in a flame. It is affected by conditions such

as the flame temperature, flame size, trajectory and size of soot within the flame. The fraction of soot escaping from the flame zone or enveloped before being oxidized results in the observed smoke (Delichatsios, 1994).

2.8.3 Toxic Products of combustion

Fire gases. Carbon dioxide and carbon monoxide are the dominant gases of combustion (Mouritz et al., 2006). During the combustion process most of the carbon is produced from smouldering, well-ventilated flaming, post-flashover fires and is converted into carbon dioxide. Carbon dioxide is commonly used to estimate burning rate because of it high yield in fires (Mulholland et al., 1991). Carbon monoxide is produced in flaming combustion but more so during smouldering combustion. However, CO production is quite slow in smouldering fires because of a lower activity in the combustion process. The production of CO is mainly a gas phase process occurring in flaming combustion (Babrauskas, 1995). The production follows a sequence of complex reactions of oxygen with carbon-containing combustion products or fuel vapour. The equivalence fuel-to-air ratio also determines the extent of CO formation (Pitts, 1994). The availability of oxygen in a fire can be lowered by the reducing the oxygen concentration in the air or by reducing the air flow rate (fed into a fire) itself. High concentration of oxygen in a fire results in an increased CO production.

The effects of toxic products. The effects of toxic fire products are not the primary focus of this study. However, it is an important fire hazard parameter related to the emission of toxins into the atmosphere. Exposure to these products of combustion has various consequences and can even lead to death or long term health complications. The amount of heat produced by combustibles and the concentration of smoke, gases and aerosols are the determinants used to categorise the extent of toxicity (Babrauskas et al., 1998, Babrauskas et al., 1992). Thermal effects can lead to skin burns, hyperthermia and respiratory tract irritation. The effects on the respiratory tract as a result of sensory irritation can compromise judgement which includes an inability to negotiate escape route while longer or higher exposures could lead to incapacitation or death (Madrzykowski and Stroup, 2008b). Smoke, as a visible fire effluent, causes obscuration making it difficult to locate escape routes (Gann et al., 1994). The inhalation of asphyxiate gases of combustion can result in the depression of the central nervous system, depending on the exposure this may lead to disorientation, unconsciousness and eventually death.

CHAPTER 3: EXPERIMENTAL

3.1 Materials and methods

The linear low density polyethylene (LLDPE) was supplied by Sasol Polymers. It was a hexene comonomer-based rotomoulding grade powder (Grade HR 411: MFI 3.5 (190°C/2.16 kg); density 0.939 g·cm^{-3}; particle size: 90% < 600 μm). Natural Zimbabwean flake graphite was obtained from BEP Bestobell, Johannesburg. Chemserve Systems supplied the release agent Sliprolease 20 K and Orchem provided the antioxidant Orox PK (polymerized 2,2,4-trimethyl-1,2-dihydroquinoline). Two grades of expandable graphite ES250 B5 (onset temperature 220°C) and ES170 300A (onset temperature 300°C) were obtained from Qingdao Kropfmuehl Graphite (China). The latter constituted the expandable form used in this study. The former could not be used for rotomoulding as the expansion onset temperature was too low.

The exfoliated graphite form was prepared by exposing the ES250 B5 grade powder to high heat for 5 minutes by placing it in a Thermopower electric furnace set at 600°C. A dry-blend formulation was prepared as follows. The exfoliated ES250 B5 (10 wt.%) and the antioxidant Orox PK (2 wt.%) were mixed with the LLDPE powder in a high speed mixer-grinder for five minutes. The same blending procedure was used to make a dry-blend containing the ES170 300A graphite. These powder mixtures were used directly to rotomould test samples. However, in all cases the antioxidant Orox PK (2 wt.%) was blended into the powders using a blender for one minute.

A slightly different procedure was used to prepare the carbon black and flake graphite composites. The filler (10 wt.% carbon black or flake graphite) was manually mixed with polyethylene powder. The samples were melt-compounded in a 40 mm co-rotating Berstorff twin screw extruder. The temperature profile, from hopper to die, was as follows:
17/175/220/225/214/234/235/233/235°C

More detail on the processing conditions were reported elsewhere (Mhike and Focke, 2013). The composite strands were water cooled, air dried and granulated into pellets. These were then milled into rotomoulding powder using a Pallmann 300 pulverizer.

A stainless steel rectangular cuboid mould with inside dimensions 200 × 150 × 100 mm was used for rotomoulding. The heat stabilizer Orox PK was blended into the powders using a blender for a period of one minute. A constant volume of material (320 cm^3) was used for all compositions in order to obtain a constant part thickness of ca. 2.7 mm. The charge mass was adjusted by considering the density of the various components. The rotomoulding machine was

a modified Thermopower convection oven that was fitted with a biaxial mould rotating mechanism. Details of the rotomoulding process parameters were previously reported (Mhike and Focke, 2013). The oven was set at 300°C, the heating time was 60 min and the rotation speed was 30 rpm. The mould was allowed to cool down inside the oven using ambient air before opening.

Composite test specimens. The linear low density polyethylene (LLDPE) composite samples containing 10 wt.% carbon or graphite filler were studied. Detailed information on the characteristics and physical properties of the composites are presented elsewhere (Mhike and Focke, 2013). However, attributes which are significant to the present study are reported here. The interest of this study was the fire behaviour of melt-compounded and rotomoulded composite samples as they differed with respect to the nature of the graphite fillers used in polyethylene. As mentioned above, the samples were prepared by rotational moulding in another study (Mhike et al., 2017).

3.2 Material characterisation

3.2.1 Thermogravimetric analysis (TGA)

Thermogravimetric analysis of the LLDPE and 10 wt.% graphite composites were acquired with a Perkin Elmer TGA 4000. Alumina pans were used to hold the samples. The samples size was approximately 48 mg. Temperature was scanned from 25 to 800°C at a rate of 10°C·min $^{-1}$ in a stream of gas, either nitrogen (10 mL·min^{-1}) or air (50 mL·min^{-1}).

3.2.2 Differential Scanning Calorimetry (DSC)

Differential scanning calorimetry was used to measure the heat flow into (endothermic) or out (exothermic) of the specimens. The exothermic and endothermic peaks reveal the crystallization and crystal melting temperatures of polyethylene composites. DSC thermographs of LLDPE and the graphite composites were acquired using a Mettler Toledo DSC 1 STAR thermal analyser in air flowing at a rate of 50 mL·min^{-1} and heating rate of 10°C·min^{-1}. Specimens of approximately 6 mg in size were first kept isothermally at -50°C for 5 min before heating to 200°C. The specimen were then kept isothermally at 200°C for 5 minutes before cooling at 10°C·min^{-1} to -50°C.

3.2.3 Fourier Transform Infrared spectroscopy (FTIR)

Fourier transform infrared spectroscopy provides information about vibrational and rotational absorption bands related to the presence of different functional groups in the organic material. This reveals information on the chemical composition. The spectra for the LLDPE and graphite composites were recorded on a PerkinElmer Spectrum 100 FTIR instrument. Small samples of the composites were melted between two glass slides placed on a hot plate. Thin microscope glass cover slides were placed on top of the bottom slide at the two ends so that the two glass slides were separated by a small gap. Once the plastic pieces were molten, the two glass slides were pushed together by placing a heavy weight on top. Spectra were recorded using the thin pressed sheets (thickness ca. 200 μm) in transmission and in the diffuse reflection (DRIFT) modes. The reported spectra represent averages of 12 scans at a resolution of 4 cm^{-1}. For the latter, a PIKE Technologies DiffusIR diffuse reflection accessory was implemented.

3.2.4 Scanning Electron Microscope (SEM)

The graphite particle morphologies were studied using a JEOL JSM 5800LV scanning electron microscope (SEM). The low resolution micrographs were captured at an acceleration voltages of 20 kV. No electro-conductive coating was applied on the graphite particles.

3.2 Fire test Methods

The main purpose of this study was to assemble and investigate the capability of the laser pyrolysis-TGA system as a prototype micro-flammability tester. The idea was that LPy-TGA could allow experimental analysis of milligram size samples. Polyethylene composites reinforced with different graphite forms at 10 wt.% were used as the sample test materials. Cone calorimeter and pyrolysis combustion flow calorimetry fire tests were done for the same composites and the results compared to those obtained with LPy-TGA.

3.2.1 Cone calorimeter

Fire tests were conducted according to the ISO 5660-1 standard on a Dual Cone Calorimeter (Fire Testing Technology (UK) Ltd.). Specimens with lateral dimensions of 100 × 100 mm with an average thickness of 2.70 ± 0.17 mm were wrapped in aluminium foil and exposed horizontally to an external heat flux of 35 kW m^{-2}. Tests were conducted in triplicate and average results are reported. The parameters recorded included time to ignition, heat release rate, mass loss rate, smoke production, and carbon monoxide and carbon dioxide production

rates. However, the present study focused on the time to ignition, heat release rate, mass loss rate and the fire hazard parameters, i.e. fire growth rate (*FIGRA*) and maximum average rate of emission (*MARHE*).

3.2.2 Pyrolysis Combustion Flow Calorimeter (PCFC)

Pyrolysis combustion flow calorimetry was performed on a Fire Testing Technology FTT Micro Calorimeter. In this system, about 5.0 mg sample was heated to 900°C at a heating rate of 1.0°C·s^{-1} in a stream of nitrogen flowing at 80 cm^3·min^{-1}. The volatile, anaerobic thermal degradation products in the nitrogen gas stream were mixed with 20 cm^3·min^{-1} stream of oxygen prior to entering a combustion furnace set at 900°C. The parameters measured by the instrument included the heat release rate (*HRR*) in kW·kg^{-1} (calculated from the measured depletion of oxygen), heat release capacity (*HRC*) in MJ·kg^{-1}·K^{-1} (obtained by dividing the sum of the peak *HRR* by the heating rate in °C·s^{-1}), the total heat release (*THR*) in MJ·kg^{-1} (determined by integrating the *HRR* curve).

3.2.3 LPy-TGA Method

The LPy-TGA experimental apparatus set-up is shown in Figure 14 together with the dimensions of the ceramic crucible used in the Perkin-Elmer TGA 4000 thermogravimetric analyser. The 6.4 mm diameter ceramic crucible was filled with a sample of polyethylene composite measuring 48 ± 2 mg in each case. The crucible was placed inside the TGA chamber on sample holder C. The chamber was heated to an isothermal temperature of 200°C to consolidate the material for 20 min under an inert (nitrogen) atmosphere. It was then allowed to cool for 20 minutes prior to the laser pyrolysis run. The TGA chamber gas flow was switched off making it to run in a normal air atmosphere. The class-4 Edinburgh PL6 10.6 µm CO_2 laser beam was monitored ahead of each pyrolysis run. The laser beam was applied to pyrolysis samples for 40 minutes. Different laser beam power levels (1.5, 2, 3 and 4 W) and initial isothermal TGA chamber temperature settings (50, 100, 150 and 200°C) were employed.

CHAPTER 4: RESULTS AND DISCUSSION

4.1 Characterisation results

Characterisation results for the carbon/graphite fillers and the corresponding polyethylene/graphite composites were reported previously (Focke et al., 2014, Mhike and Focke, 2013, Mhike et al., 2017). Table 1 and Table 2 present thermal conductivity of composites and physical properties of different graphite types including mean particle size, BET surface area and density. The particle size distributions for different types of graphite fillers are shown in Figure 15.

Table 1: Room temperature thermal conductivity (*k*) of the rotomoulded polyethylene-graphite composites

Sample	κ, $W \cdot m^{-1} \cdot K^{-1}$
Neat LLDPE	0.42 ± 0.01
Carbon black	0.38 ± 0.01
Expandable graphite	0.57 ± 0.02
Exfoliated (Expanded) graphite	0.68 ± 0.02
Zimbabwean Flake graphite	0.56 ± 0.00

Table 2: Mean particle size, surface area and density of the various graphite filler types

Graphite type	d_{50}, μm	Surface area, $m^2 \cdot g^{-1}$	Density, $g \cdot cm^{-3}$
Flake graphite	112	4.0	2.34
Expandable graphite ES250 B5	381	2.4	2.08
Exfoliated graphite ES250 B5	-	16.3	0.66
Expandable graphite ES170 300A	521	2.09	2.23

Zimbabwean flake graphite particle size d_{50} was much lower compared to expanded and expandable graphite. XRF (Mhike and Focke, 2013) results showed that the carbon content of the Zimbabwean flake graphite was about 92 wt.%. Silica and clay minerals were present as impurities. The carbon content was 90 wt.% and 80 wt.% for expandable graphite ES250 B5 and ES170 300A respectively.

Table 2 lists the thermal conductivities of the polyethylene/graphite composites as measured at ambient conditions. Incorporation of graphite fillers at 10 wt.% enhanced the thermal conductivity by at least 33%. However, the highest conductivity found was only 0.68 $W \cdot m^{-1} \cdot K^{-1}$ for the exfoliated graphite composite. This composite also featured a low electrical resistivity and therefore good antistatic performance (Mhike and Focke, 2013). This was attributed to presence of interconnected particle clusters that were observable in both optical and SEM micrographs of the composites reported elsewhere (Mhike and Focke, 2013). It is known that dispersion states in which graphite particles form conductive chains also results in composites with higher thermal conductivities.(Agari et al., 1991)

Figure 17 shows DSC heating and cooling results for polyethylene/graphite composites. The higher crystallisation temperatures of the polyethylene composites are due to a nucleating provided by the graphite fillers.

FTIR and DRIFT results in Figure 18, Figure 19 and Figure 20 suggest that the dominant mechanism during laser pyrolysis was photothermal in nature because of the very high absorption values.

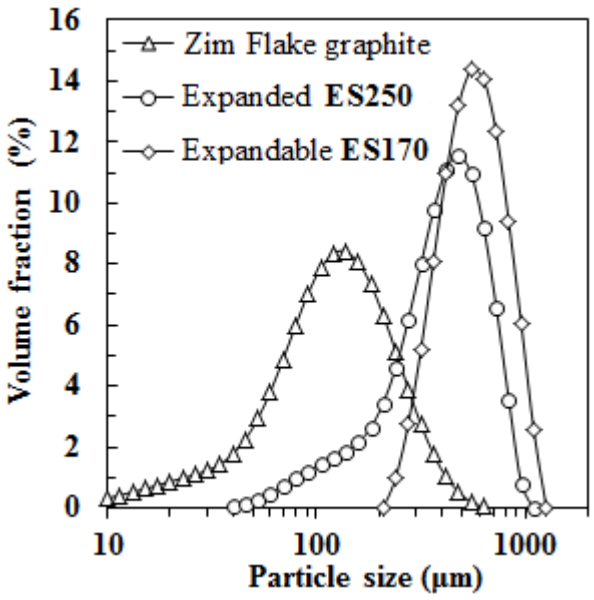

Figure 15: Graphite particle size distributions

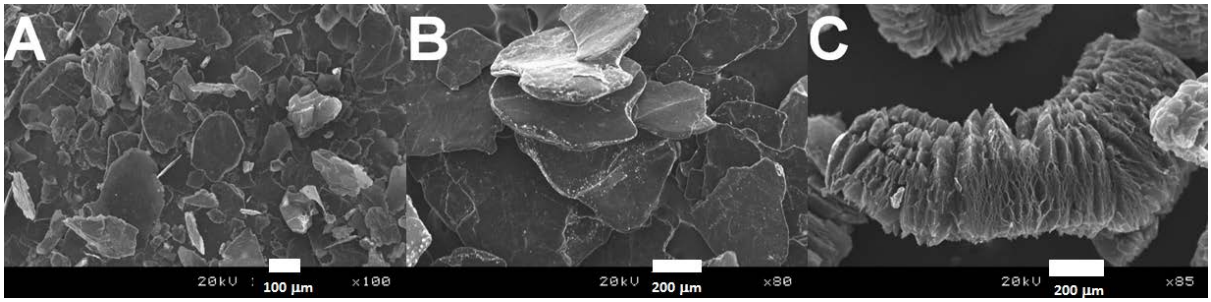

Figure 16: SEM micrographs of the flaky nature of (A) flake graphite, (B) expandable graphite (ES170), and (C) the 'worm-like structure' of exfoliated graphite (ES250 B5).

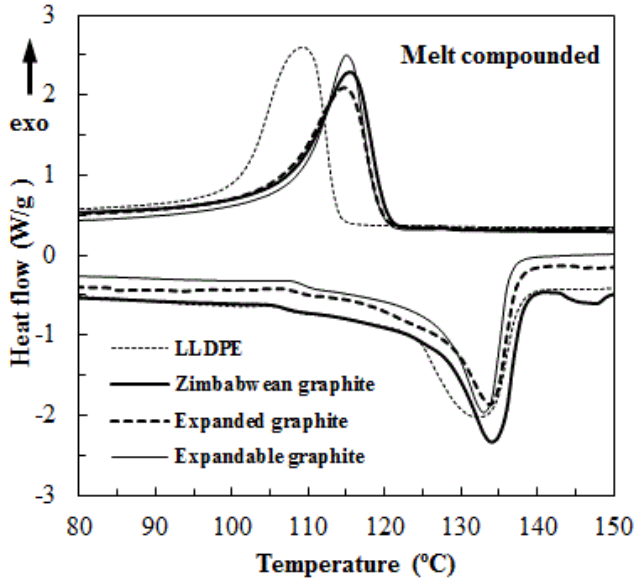

Figure 17: DSC results for melt-compounded rotomoulded polyethylene/graphite composites.

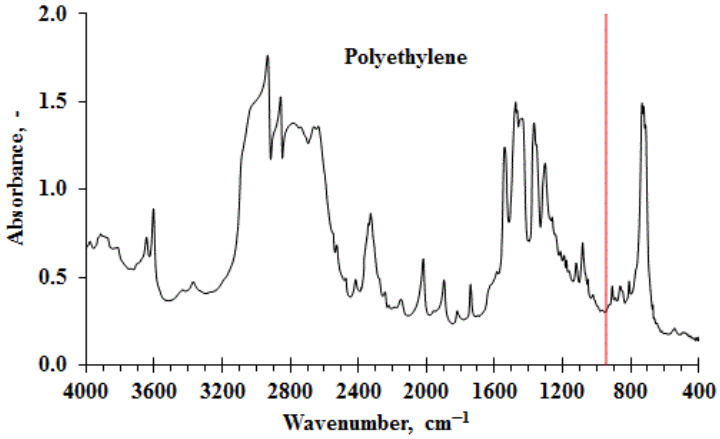

Figure 18: FTIR spectra of polyethylene, where red line signifies absorption fraction of laser light wave length 944cm^{-1} by polyethylene which is equivalent to 10.6µm CO_2 continuous wave laser.

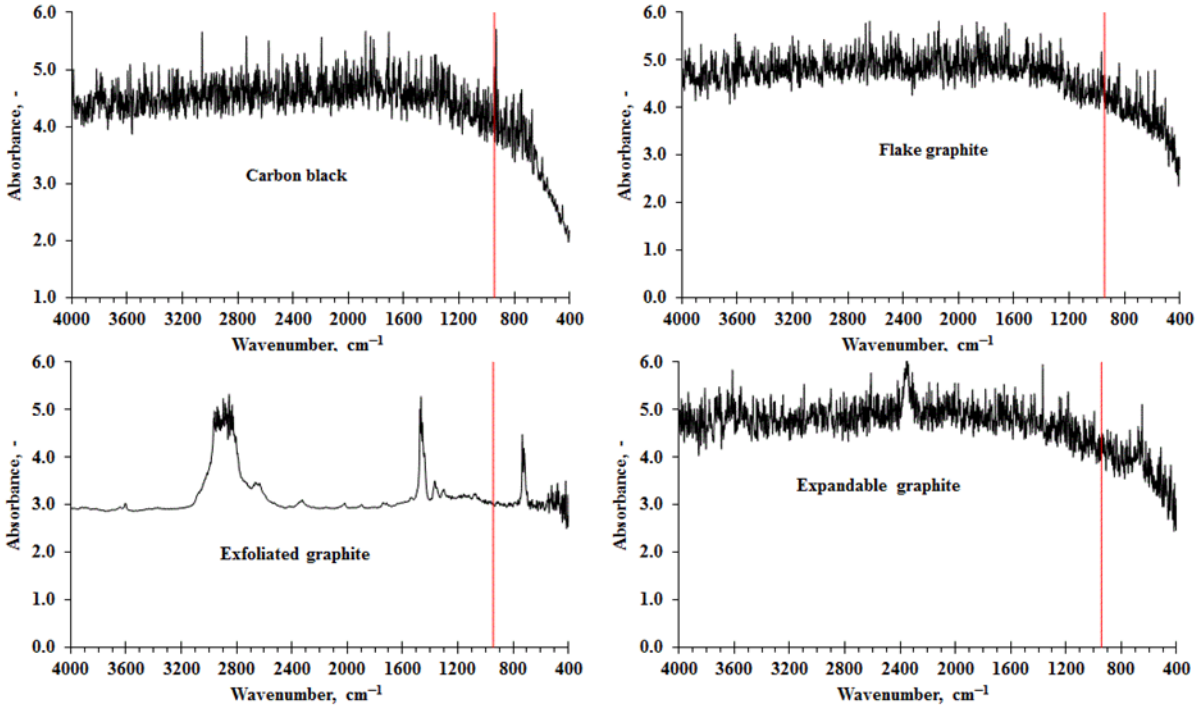

Figure 19: FTIR spectra of polyethylene composites with 10 wt.% of carbon black, flake graphite, exfoliated graphite and expandable graphite, where the red line signifies absorption fraction of laser light wave length 944 cm^{-1} by the composites which is equivalent to 10.6 µm CO_2 continuous wave laser.

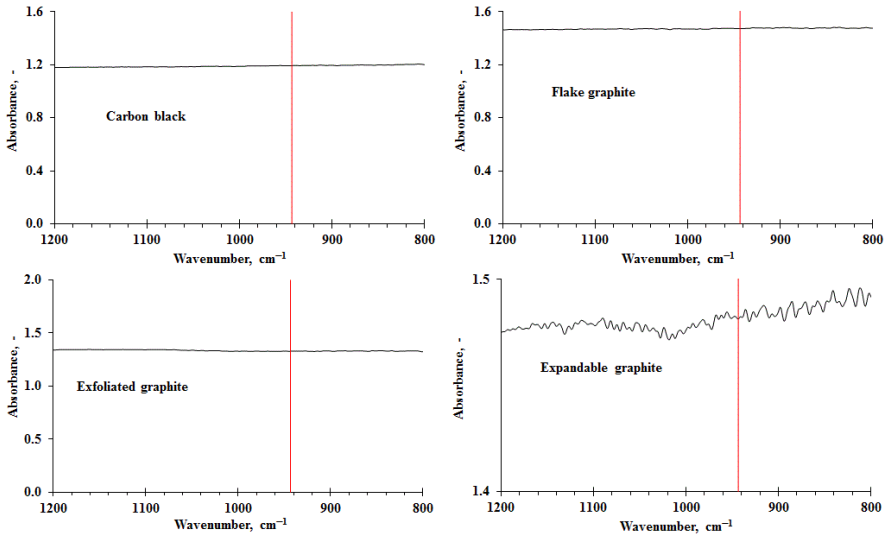

Figure 20: The diffuse reflection infrared spectra (DRIFT) of polyethylene composites with 10 wt.% of carbon black, flake graphite, exfoliated graphite and expandable graphite, where the red line signifies absorption fraction of laser light wave length 944 cm^{-1} by the composites which is equivalent to 10.6µm CO_2 continuous wave laser.

4.2 Thermogravimetric analysis (TGA)

Figure 21 shows thermogravimetric data obtained in an inert nitrogen atmosphere showing the pyrolysis of polyethylene and the graphite composites. The neat polyethylene started to loose mass at 400°C and the mass loss was complete at about 500°C. Similar trends were found for all the other compounds. However, the carbon black compound was the least stable while the expandable graphite showed the slowest mass loss. The flake graphite filler was stable at the decomposition temperature of polyethylene. The graphite fillers are not expected to affect the pyrolysis reaction rates that occur in the polyethylene matrix (Mhike et al., 2015a). Instead, the slightly reduced mass loss is probably caused by the flakes acting as mass transport barriers.

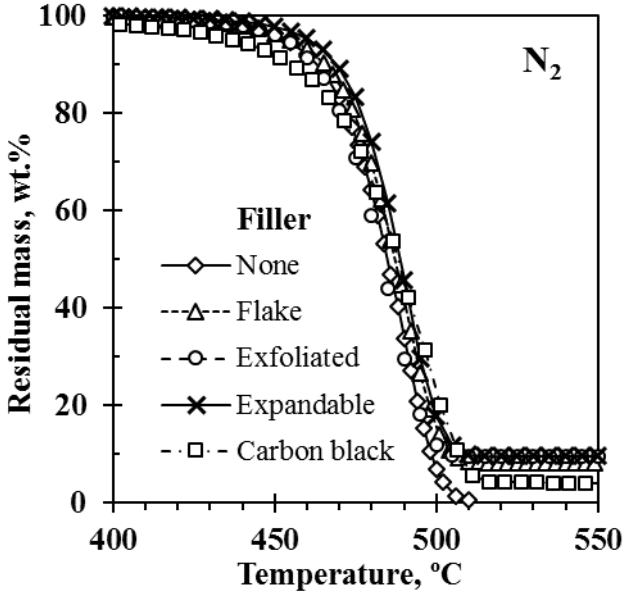

Figure 21: Thermogravimetric analysis curves obtained in nitrogen for rotomoulded LLDPE and its composites containing 10 wt.% graphite fillers. The residue remaining at 600°C were as follows: Carbon black: 2.4 wt.%; flake graphite: 9.0 wt.%; exfoliated graphite: 9.4 wt.%, and expandable graphite: 9.5 wt.%.

4.3 Cone calorimeter

Results for the cone calorimeter testing were previously reported in considerable detail as part of a separate study (Mhike et al., 2015b). The present discussion will be limited to the most important results. Table 3 and Figure 22 show representative cone calorimeter test results. The cone calorimeter data gathered for the neat polyethylene samples were suspect and, with the exception of the ignition time, they are not reported.

The shape of heat release rate (*HRR*) curves, for thermally thin samples, features a single sharp peak as the whole sample is pyrolyzed almost at once (Schartel and Hull, 2007b).

In contrast the *HRR* curve for a thermally thick, char-producing sample typically shows a rapid rise to a plateau value that is maintained as the sample is progressively consumed (Schartel and Hull, 2007b). With the exception of the expandable graphite composite, all the heat release curves plotted in Figure 22 exhibited a shape indicative of thermally thin samples.

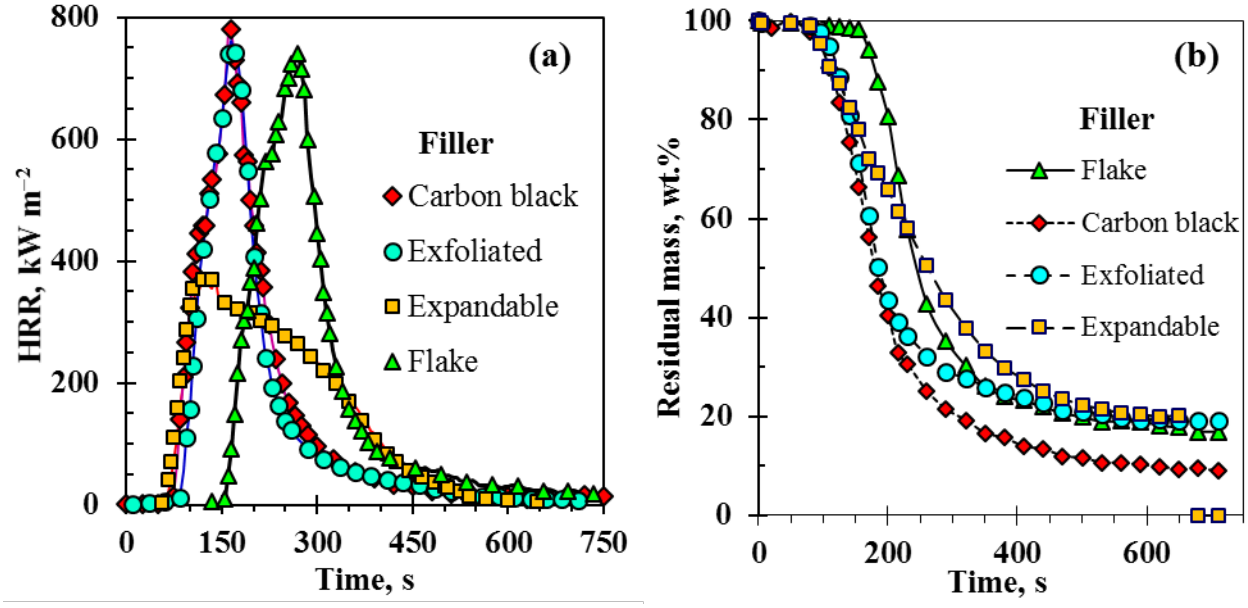

Figure 22: Typical cone calorimeter (a) heat release rate (*HRR*) and (b) mass loss curves of rotomoulded polyethylene/graphite composites. The sample sheets were backed by aluminium foil and their dimensions were 100 mm × 100 mm × 2.7 mm. They were mounted horizontally and exposed from above to an external heat flux of 35 kW·m^{-2}.

The *HRR* curve for the expandable graphite composite featured a more flattened shape. It also exhibited the lowest peak heat release rate (*pHRR*) of 360 ± 10 kW·m^{-2} of all samples tested (Figure 22 and Table 3). Both observations can be explained by a protective barrier layer formed at the top surface of the sample by 'worm like' structures resulting from the endothermic expansion of the EG (Figure 16C). This barrier slowed down heat transfer into the substrate during the cone calorimeter testing. The data in Table 3 also shows that the *pHRR* was basically the same whether the composites contained carbon black, flake graphite or exfoliated graphite as filler. The mean peak heat release rates for these composites, taken together, was 763 ± 43 kW·m^{-2}.

The times to ignition of the carbon black and expandable graphite composites were also statistically indistinguishable and taken together it was 54 ± 10 s. The value for the exfoliated graphite was a little higher (77 ± 7 s). Rather unexpectedly the flake graphite composite

featured a significantly longer ignition delay of 150 ± 11 s. This was more than 80% longer than the value recorded for the other samples.

The fire growth rate (*FIGRA*) and the maximum average rate of heat emission (*MARHE*) are indices that may be used to interpret cone calorimeter data.(Schartel and Hull, 2007b, Sacristán et al., 2010) The *FIGRA* is an estimator for the fire spread rate and size of the fire whereas the *MARHE* guesstimates the tendency of a fire to develop.(Sacristán et al., 2010) The *FIGRA* is defined as the maximum quotient of $HRR(t)/t$, i.e. the heat release rate up to a time t divided by this time. Usually it can be estimated using the following expression

$$\boldsymbol{FIGRA = pHRR/time\ to\ pHRR} \tag{4.1}$$

Table 3 also reports the *FIGRA* and *MARHE* indices. The values of the neat LLDPE could not be determined as it dripped and the melt flowed away during the cone calorimeter tests. The *FIGRA* was expected to be higher as it contained more fuel than the filled compounds. The graphite fillers are stable to very high temperatures and therefore reduce the effective solid fuel content. Compared to the carbon black and exfoliated graphite composites, the flake graphite and expandable graphite composites exhibited the lowest *FIGRA* and *MARHE* values. The flake graphite composite had the lowest *MARHE* of 222 $kW \cdot m^{-2}$. This suggests that it had the lowest propensity of developing into a fire.

Both the *FIGRA* and *MARHE* indices are attempts to capture cone calorimeter performance with a single quantifiable parameter. However, this naïve approach that can lead to erroneous conclusions (Schartel and Hull, 2007b). It would certainly be better to consider the two most important parameters pertinent to fire hazards, i.e. the fire load and flame spread, simultaneously (Schartel and Hull, 2007b). The fire load is the total amount of heat that can be produced by a flammable material once it is ignited. In the cone calorimeter this index is quantified by the total heat released (*tHR*) during the cone calorimeter test.

However, the flame spread rate is not directly determined in a cone calorimeter. Petrella (Petrella, 1994) proposed the fire growth index ($pHRR/t_{ig}$) as an estimator of the flame spread instead of the *FIGRA*. The Petrella plot helps to visualize the effect of a flame retardant on the magnitude of both fire hazard parameters.(Schartel and Hull, 2007b, Petrella, 1994) It is a plot of the total heat released *tHR* (as the fire load) against $pHRR/t_{ig}$ (as a fire growth index). For a material to be effectively flame retarded both the fire load and the fire growth index should assume low values. According to the Petrella plot of Figure 23, the flake graphite composite

gave a slightly higher fire load in the present cone tests compared to the other samples while the carbon black composite exhibited the highest fire growth index. The flake graphite composites exhibited the lowest fire growth index mainly because of a longer time to ignition. In contrast, for the expandable graphite composite the reduction of this parameter was mainly due to a reduction in the *pHRR*. To see this, please refer to Equation 1 and Figure 23.

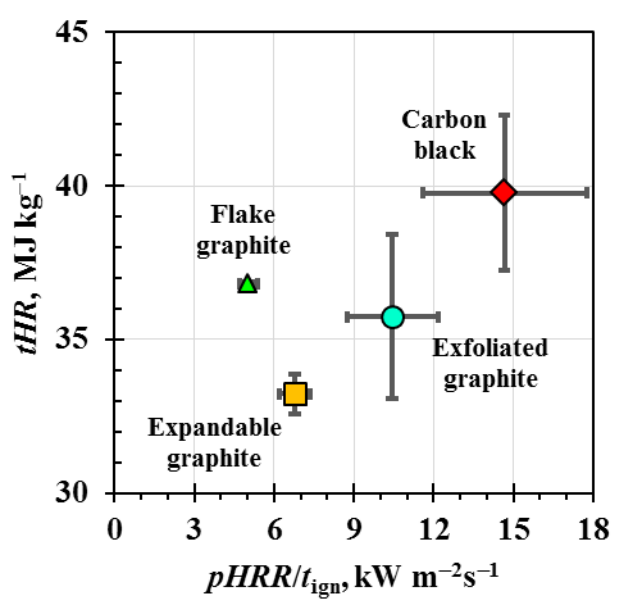

Figure 23: Petrella plot for the rotomolded polyethylene/graphite composites. The sample sheets were backed by aluminium foil and their dimensions were 100 mm × 100 mm × 2.7 mm. They were mounted horizontally and exposed from above to an external heat flux of 35 kW m^{-2}.

Figure 22(b) compares representative mass loss curves obtained during cone calorimeter testing. The expandable graphite composite featured a reduced mass loss rate compared to the other composites. For the flake graphite composite there is also a significant delay before mass loss proceeds in the trace. This parallels the observed delay in the heat release and also accords with the longer ignition time found for this material. For all practical purposes, Figure 24 shows that there is a nearly perfect correlation between mass loss and heat release. In other words, the pyrolysis-gasification of the LLDPE was independent of the degree of conversion and was not affected by any of the carbon-based additives. The implication is that the heat release rates are directly proportional to the time derivative of the mass loss curves and can therefore be estimated from those curves. Previous work has already shown that heat release rate has a linear relationship with mass loss rate and carbon dioxide evolution (Mouritz et al., 2006). Hence, mass loss rate can be used to predict heat release rate if the effective heat

of complete combustion of a material is known. Therefore, the slope of the mass loss curve indicates the mass loss rate (*MLR*) and it should correspond well with both the *MLR* and *HRR* curves obtained in the fire tests.

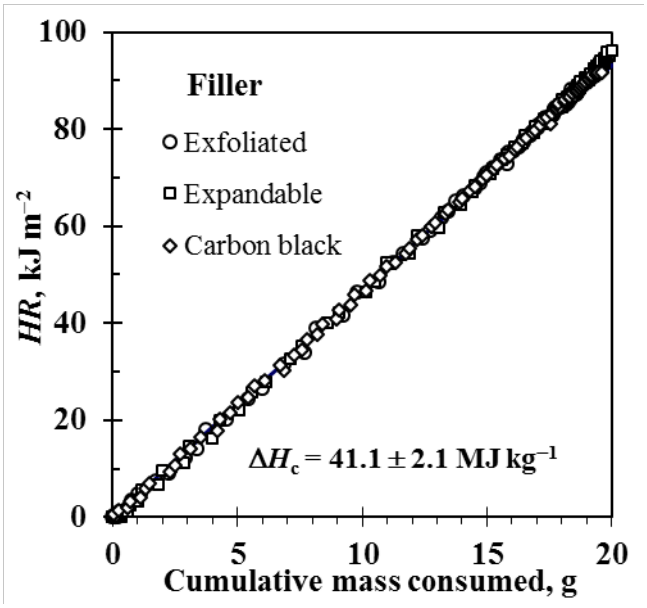

Figure 24: Cumulative heat release (*HR*) as a function of cumulative mass loss in cone calorimeter tests conducted on rotomoulded polyethylene/graphite composites. The sample sheets were backed by aluminium foil and their dimensions were 100 mm × 100 mm × 2.7 mm. They were mounted horizontally and exposed from above to an external heat flux of 35 kW m^{-2}.

Table 3: Times to ignition (t_{ig}), peak heat release rates (*pHRR*), fire growth rates (*FIGRA*) and the maximum average rate of heat emission (*MAHRE*) of polyethylene/graphite composites

Composite	t_{ign}, s	*pHRR*, kW·m^{-2}	*FIGRA*, kW·$m^{-2}s^{-1}$	*MAHRE*, kW·m^{-2}
Neat LLDPE	82 ± 10[#]	-	-	-
Carbon black	54 ± 14	758 ± 20	5.0 ± 0.2	328 ± 14
Expandable graphite	53 ± 6	360 ± 10	2.9 ± 0.3	217 ± 5
Exfoliated graphite	77 ± 7	793 ± 55	5.0 ± 0.8	292 ± 8
Flake graphite	150 ± 11	725 ± 23	2.7 ± 0.0	191 ± 65

[#] The ignition time are questionable as the sample melted and material flowed away.

4.4 Pyrolysis Combustion Flow Calorimeter

Pyrolysis combustion flow calorimetry (PCFC) results are summarised in Table 4 and representative heat release rate curves (*HRR*) are shown in Figure 25. This bench-scale flammability test has been recommended as a screening test and for research purposes (Lyon and Walters, 2004, Susott et al., 1979). This instrument also relies on oxygen consumption calorimetry to determine heat release characteristics of a material. It separately seeks to reproduce the solid state and gas phase processes occurring in flaming combustion in a non-flaming test. The sample is thermally decomposed in an inert nitrogen gas stream by controlled heating in a pyrolysis chamber. The evolved gases are oxidized in excess oxygen in a combustion chamber at a temperature of 900 °C. The heat release rate is then inferred from the gas flow rates and the oxygen concentration measurements.

The peak heat release rates listed in Table 3 are very similar. The highest and lowest values correspond to the carbon black and the exfoliated graphite samples respectively. However, the difference is only about 7.4 %. This is in stark contrast with the cone calorimeter data where more significant differences were observed. In addition, in that case the highest and lowest values were for the exfoliated and expandable graphite samples respectively with the latter equal to only 55 % of the former.

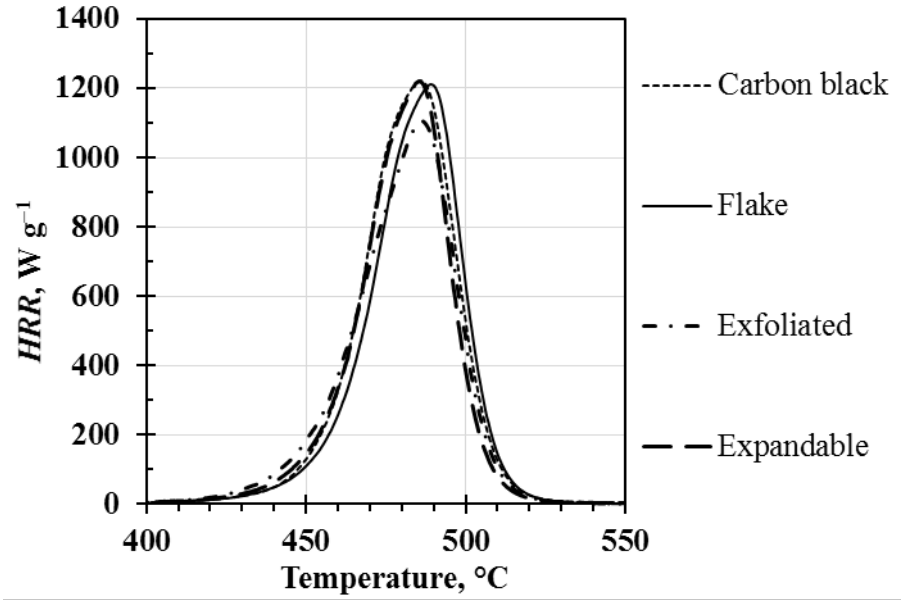

Figure 25: Pyrolysis combustion flow calorimeter (PCFC) results obtained on rotomoulded polyethylene/graphite composite samples.

Table 4: Summary of pyrolysis combustion flow calorimeter results obtained for the polyethylene/graphite composites (*HRR*) in W g^{-1} (calculated from the measured depletion of oxygen), heat release capacity (*HRC*) in MJ·kg^{-1}·K^{-1} (obtained by dividing the sum of the peak *HRR* by the heating rate in K·s^{-1}), the total heat release (*THR*) in MJ·kg^{-1}

Sample	Residue [wt.%]	T_p [°C]	*pHRR* [MW kg^{-1}]	*THR* [MJ kg^{-1}]	*HRC* [MJ kg^{-1} K^{-1}]
LLDPE	None	486.9±1.2	1.223±0.008	43.9±0.2	1.253±0.012
Carbon black	4.65±0.07	488.4±1.8	1.216±0.008	41.8±0.8	1.239±0.008
Flake graphite	7.80±0.19	489.0±0.7	1.209±0.004	40.8±0.2	1.230±0.003
Exfoliated graphite	7.79±0.20	487.3±1.5	1.131±0.019	40.7±0.6	1.151±0.024
Expandable graphite	8.45±0.32	487.0±1.2	1.206±0.010	40.5±0.2	1.223±0.006

Table 4 shows that the thermal decomposition let to char fraction that mirrored the trends observed in the TGA data and in the cone calorimeter results. Figure 25 shows that the pyrolysis, releasing a volatile fuel, occurred in a single step. In such cases the maximum specific heat release rate of the sample is related to the pyrolysis kinetic parameters at a constant heating rate of β = 1.0 K·s^{-1} (Lyon, 2000a):

$$HRC = pHRR/\beta = (1-\mu)\Delta H_c E_a / (eRT_p^2) \qquad (4.2)$$

where *HRC* is the heat release capacity; E_a is the activation energy for pyrolysis; T_p is the temperature of maximum mass loss rate; *e*, *R* are the natural number and gas constant, respectively, μ is the inert residue, and ΔH_c is the heat of combustion of the fuel gases per unit initial mass of solid and it depends only on the composition of the material (Lyon, 2000a). Lyon and Walters (Lyon and Walters, 2004) declare that the heat release capacity is a reliable indicator of fire hazard. This parameter spans two orders of magnitude from 13 J·kg^{-1}·K^{-1} for polyimide to 1676 J·kg^{-1}·K^{-1} for polypropylene (Lyon and Walters, 2004).

The differences in the heat release capacities of the different samples listed in Table 4 are not statistically significant. The same is true for the peak temperatures. These observations suggest that none of the fillers affected the decomposition behaviour of the matrix polymer under homogeneous pyrolysis conditions. This is supported by the fact that the total heat release (*tHR*), corrected for the amount of polymer present in the sample, was essentially the same for all the compounds, and equal to 42.1 ± 0.2 kJ·kg^{-1}.

4.5 Laser pyrolysis -TGA

Laser pyrolysis experiments were conducted at different laser power densities and initial oven temperature settings. The full results are presented in Appendix IV. A striking feature is the considerable scatter in- and overlap of the collected data. This made reliable quantification and rational interpretation very difficult. Nevertheless, some general trends are noticeable. Figure 26 show mass loss and temperature data collected at an initial oven temperature of 100°C and laser power settings of 1.5, 2.0 and 3.0 W. These power settings correspond to IR heat fluxes of approximately 46, 62 and 93 $kW \cdot m^{-2}$. These values are in the range used in conventional cone calorimetry testing. Data obtained for a power setting of 1 W, corresponding to a heat flux of 31 $kW \cdot m^{-2}$ are not shown as only the carbon black compound showed a rather small mass loss over time. At an IR heat flux of 46 $kW \cdot m^{-2}$, only the carbon black and the expandable graphite composites showed mass loss over time (Figure 26(a)). The other samples just showed an initial small drop in mass. This occurred within the first few minutes of irradiation but afterwards the mass remained stable. These observations are in stark contrast with the results obtained during the cone calorimeter tests. In those experiments major mass loss took place inside 20 min at a heat flux of just 35 $kW \cdot m^{-2}$.

Figure 26 shows that the thermocouple located just below the crucible detected a significant rise in temperature within minutes of irradiation by the laser, irrespective of the applied laser power. Beyond about five minutes the temperatures stabilized at plateau values that differed depending on the sample nature and the applied laser power. The temperature data shows considerable scatter but the trend indicated is that higher temperatures were recorded for those samples that showed higher mass loss and lower temperatures were recorded for those compounds that show slower mass loss. Also, the temperature plateau values increased with increasing laser power. The lowest increase reported in Figure 26 is ca. 25°C for the flake graphite compound at 46 $kW \cdot m^{-2}$. The highest reported in Figure 26 exceeds 55°C for carbon black at a laser power setting of 3 W (equivalent to 93 $kW \cdot m^{-2}$). However, as the laser power was increased, the mass loss rate increased too. At a laser power of 2 W (62 $kW \cdot m^{-2}$), the flake graphite showed the lowest mass loss rate and the lowest plateau temperatures. This apparent stability probably indicates that the flake graphite effectively reflected the incoming radiation. Less radiation was absorbed and therefore the sample temperature remained lower than that of the other compounds. This effect probably extends to the temperature at the top surface of the sample, which if it had been lower, would have result in a lower rate of vaporization driven by pyrolysis. Interestingly the expandable graphite performed worst in the LPy-TGA test whereas

it performed best in the cone calorimeter tests. This can be rationalized as follows. During the LPy-TGA tests, the expandable graphite foamed up and formed a loose structure that was heated throughout to a higher temperature than the other samples (Figure 26(d)). This means that it pyrolyzed faster as indicated by the faster mass loss.

At a laser power setting of 3 W (93 $kW \cdot m^{-2}$) the flake graphite still performed best but now the carbon black sample lost mass faster than the expandable graphite. However, all samples show quite rapid mass loss. Except for the carbon black compound, the residue level approached about 10 wt.% as expected.

Simulations conducted with the ThermaKin numerical pyrolysis software, previously reported for cone calorimetry conditions (Mhike et al., 2015b), indicated that it was the reflectivity of the flake graphite that provided a measure of fire protection. It is therefore likely that this was also the case in the LPy-TGA experiments where the flake graphite provided superior protection against thermal degradation induced by the IR laser compared to the compounds filled with carbon black, exfoliated and expandable graphite.

4.6 Preliminary result on how to employ the laser pyrolysis equation

As an example we have fitted equation 2.3 to two samples only: (1) LLDPE with 10% Zimbabwe flake graphite and (5) pure LLDPE. One can clearly see that addition of some 10% flake graphite to the LLDPE make the material more resilient to the laser beam. This evidence from (a) the additional time of about 0.3 minutes from the start of the laser irradiation during which no mass is lost (b) the much lower slope in curve (1) than in curve (5) an indication of more residual mass for the composited LLDPE than the pure counterpart. The fittings for the two materials have yielded the parameters listed in Table 1 where one notes that the composite has a higher enthalpy change (ΔH) than the pure LLDPE, an indication that it take a lot more energy to change the chemical identity of the composite than the pure one. Also the specific heat is greatly improved after additives–from 62 to 505 $J \cdot kg^{-1} \cdot K^{-1}$. Materials with high specific heat capacity require more energy to heat them up which may mean more resilience to fire sources as is the case of water which has a specific heat capacity of 4200 $J \cdot kg^{-1} \cdot K^{-1}$.

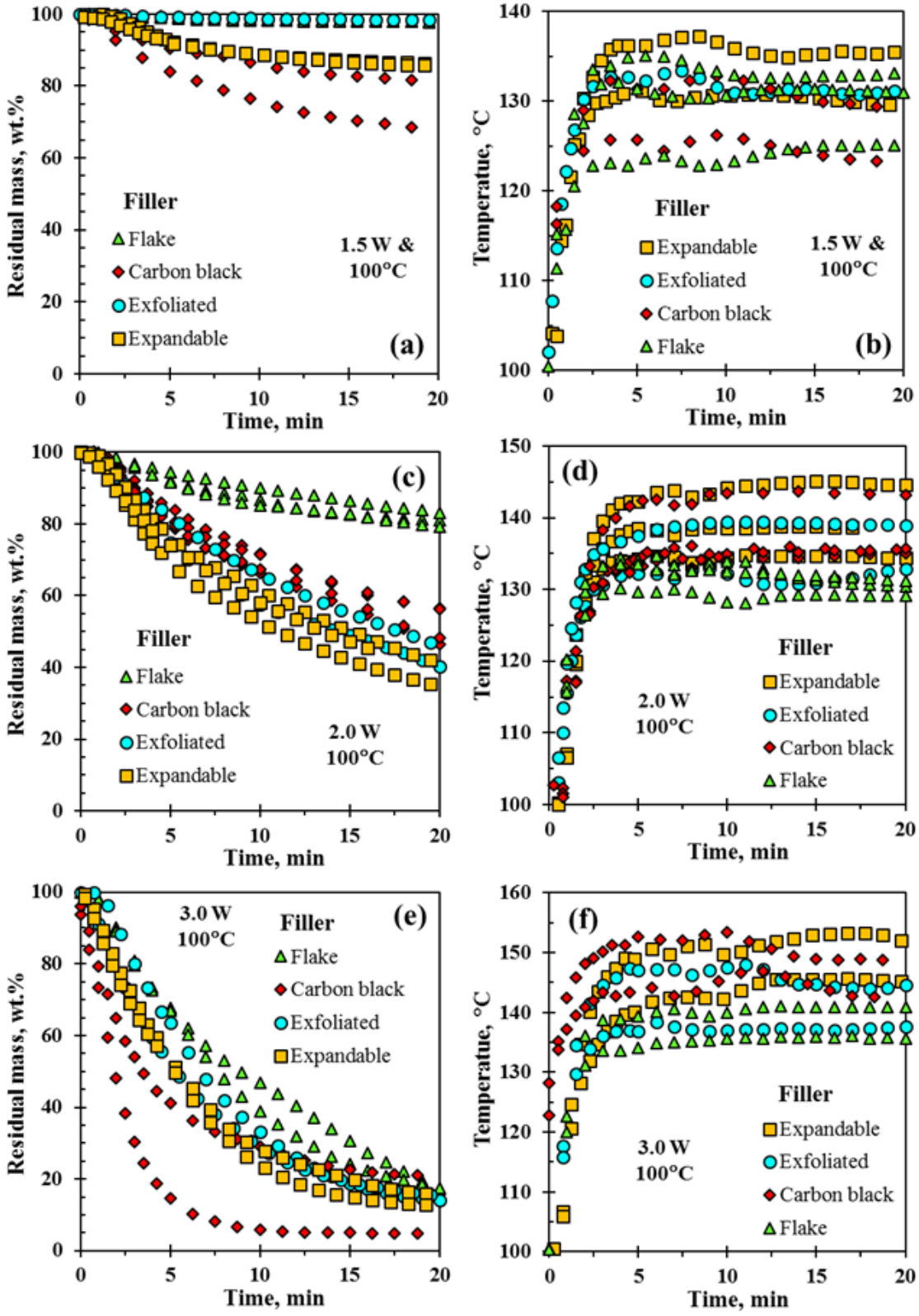

Figure 26: Flake graphite (FG), Carbon black (CB), Exfoliated graphite (XG), Expandable graphite (EG) LPy-TGA results of mass loss at 100°C TGA isothermal temperature with (a) 1.5 W; (b) 2 W, and (c) 3 W laser beam power.

CHAPTER 6: CONCLUSIONS

The thermal response of linear low density polyethylene compounds, containing 10 wt.% of different carbon-based fillers cf. carbon black, natural flake graphite, exfoliated graphite and expandable graphite was studied in cone calorimeter fire testing, pyrolysis combustion flow calorimetry (PCFC) and laser pyrolysis-thermogravimetric analysis (LPy-TGA). In cone calorimetry the expandable graphite proved to be an effective flame retardant by reducing the peak heat release rate by ca. 50% compared to the other compound. However, the flake graphite increased the ignition time by more than 80%, and this was attributed to the high reflectivity of this carbon form. All the compounds showed similarly (poor) fire performance results in pyrolysis combustion flow calorimetry testing. This could have been expected because the purely physical fire protection mechanisms offered by these additives are negated in this test. For flake graphite and the expandable graphite it is the reflection of incoming radiation and the formation of a thermal insulating foam at the surface of the material, respectively. The flake graphite showed the lowest mass loss in LPy-TGA testing and this is attributed to the same reflectivity effect. Surprisingly, the expandable graphite performed poorly in LPy-TGA. It is speculated that this was caused by a low absorption of the infrared laser light that resulted in the heating of all of the material at once. This caused complete foaming of the sample with subsequent pyrolysis of the porous structure. These results indicate that there are problems associated with small-scales evaluation of fire performance with current approaches. This is particularly true for flame retardants that rely on an interface mechanism where the sample aspect ratio and orientation to the heat source are important.

In conclusion, small-scale flammability tests, such as pyrolysis combustion flow calorimetry and laser pyrolysis-thermogravimetric analysis, do not reproduce cone calorimetry results when the flame retardant mechanisms rely on either the generation of barrier layers or on the reflection of incoming thermal radiation.

REFERENCES

AGARI, Y., UEDA, A. & NAGAI, S. 1991. Thermal conductivities of composites in several types of dispersion systems. *Journal of Applied Polymer Science*, 42, 1665-1669.

ANON. 2001. Thermogravimetric analysis with laser heating. *Tech Briefs* [Online]. Available: https://www.techbriefs.com/component/content/article/tb/techbriefs/physical-sciences/7314.

ASTM, S. 1999. Standard test method for heat and visible smoke release rates for materials and products using an oxygen consumption calorimeter. *E1354-99*.

BABRAUSKAS, V. 1983. Estimating large pool fire burning rates. *Fire technology,* 19, 251-261.

BABRAUSKAS, V. 1984a. *Bench-scale methods for prediction of full-scale fire behavior of furnishings and wall linings*, Society of Fire Protection Engineers Boston, MA, USA.

BABRAUSKAS, V. 1984b. Development of the cone calorimeter—a bench-scale heat release rate apparatus based on oxygen consumption. *Fire and Materials,* 8, 81-95.

BABRAUSKAS, V. 1995. The generation of CO in bench-scale fire tests and the prediction for real-scale fires. *Fire and Materials*, 19, 205-213.

BABRAUSKAS, V. 2016a. The cone calorimeter. *SFPE Handbook of Fire Protection Engineering.* Springer.

BABRAUSKAS, V. 2016b. Heat release rates. *SFPE handbook of fire protection engineering.* Springer.

BABRAUSKAS, V., GANN, R. G., LEVIN, B. C., PAABO, M., HARRIS, R. H., PEACOCK, R. D. & YUSA, S. 1998. A methodology for obtaining and using toxic potency data for fire hazard analysis. *Fire Safety Journal*, 31, 345-358.

BABRAUSKAS, V., GRAYSON, S.J.,. Heat Release Test Methods. *In:* VYTENIS BABRAUSKAS, R. G., STEPHEN GRAYSON, ed. Hazards of Combustion Products, November 2008 The Royal Society, London. Fire Science and Technology Inc.

BABRAUSKAS, V., HARRIS, R.H. JR., BRAUN, E., LEVIN, B., PAABO, M., GANN, R.G. January 1991. The Role of Bench-Scale Test Data in Assessing Real-Scale Fire Toxicity. *National Istitute of Standards and Technology (NIST) Technical Note 1284*.

BABRAUSKAS, V., LEVIN, B. C., GANN, R. G., PAABO, M., HARRIS, R. H., PEACOCK, R. D. & YUSA, S. 1992. Toxic potency measurement for fire hazard analysis. *Fire technology*, 28, 163-167.

BABRAUSKAS, V. & PEACOCK, R. D. 1992. Heat release rate: The single most important variable in fire hazard. *Fire Safety Journal*, 18, 255-272.

BABRAUSKAS, V., PEACOCK, R.D. 1991. Heat Release Rate: Single Most Important Variable in Fire Hazards. *Fire Safety Journal (1992)*, 18, 255-272.

BART, J. 2006. *Plastics additives: advanced industrial analysis*, IOS Press.

BART, J. C. 2005. *Additives in polymers: Industrial analysis and applications*, John Wiley & Sons.

BEJI, T. 2009. *Theoretical and experimental investigation on soot and radiation in fires.* University of Ulster.

BEJI, T., ZHANG, J., YAO, W. & DELICHATSIOS, M. 2011. A novel soot model for fires: validation in a laminar non-premixed flame. *Combustion and Flame*, 158, 281-290.

BERGER, C. L. & RERO, J. 2006. Understanding materials flammability. *Flammability Testing of Materials Used in Construction, Transport and Mining*, 1.

BEYLER, C. L. & HIRSCHLER, M. M. 2002. Thermal decomposition of polymers. *SFPE handbook of fire protection engineering,* 2, 111-131.
BITEAU, H., STEINHAUS, T., SCHEMEL, C., SIMEONI, A., MARLAIR, G., BAL, N. AND TORERO, J.L., Sep-2008. Calculation Methods for the Heat Release Rate of Materials of Unknown Composition. *Fire Safety Science,* 9, 1165-1176. doi:10.3801/IAFSS.FSS.9-1165.
BOND, T. C. & BERGSTROM, R. W. 2006. Light absorption by carbonaceous particles: An investigative review. *Aerosol science and technology,* 40, 27-67.
BOURBIGOT, S., LE BRAS, M., DABROWSKI, F., GILMAN, J.W., KASHIWAGI,T., 2000. PA-6 Nanocomposite Hybrid as Char Forming Agent in Intumescent Formulations. *Fire Mater.*, 24, 201-208
BOURBIGOT, S., LE BRAS, M., DUQUESNE, S., ROCHERY, M., 2004. Recent Advances for Intumescent Polymers. *Macromol Mater. Eng,* 289, 499-511.
CARPENTER, K., HUCZEK, J., JANSSENS, M. & MILLER, M. 2005. Development of a method to assess the hazard of plastic components to passengers trapped in post-collision motor vehicles fires. SAE Technical Paper.
CLARKE III, F. B. & OTTOSON, J. 1975. Fire death scenarios and firesafety planning. *Chemical and Engineering News,* 53.
DELICHATSIOS, M. 1994. A phenomenological model for smoke-point and soot formation in laminar flames. *Combustion Science and Technology,* 100, 283-298.
DI BLASI, C. 1993. Modeling and simulation of combustion processes of charring and non-charring solid fuels. *Progress in Energy and Combustion Science,* 19, 71-104.
DIGUISEPPI, C., ROBERTS, I. & LI, L. 1998. Smoke alarm ownership and house fire death rates in children. *Journal of Epidemiology and Community Health,* 52, 760.
DINENNO, P. J. 2008. *SFPE handbook of fire protection engineering*, SFPE.
DRYSDALE, D. 1998. Ignition: The Initiation of Flaming Combustion, in "An Introduction to Fire Dynamics". John Wiley & Sons Ltd, England.
E176-04, A. 2004. Standard Terminology of Fire Standards. *ASTM International*.
EMMONS, H. W. 1992. The Fractional Effective Dose Model for Assessment of Toxic. *Advances in Combustion Toxicology,* 3, 126.
FANTER, D. L., LEVY, R. L. & WOLF, C. J. 1972. Laser pyrolysis of polymers. *Analytical Chemistry,* 44, 43-48.
FOCKE, W. W., BADENHORST, H., MHIKE, W., KRUGER, H. J. & LOMBAARD, D. 2014. Characterization of commercial expandable graphite fire retardants. *Thermochimica Acta,* 584, 8-16.
FRIEDMAN, R. 1998. *Principles of fire protection chemistry and physics*, Jones & Bartlett Learning.
GANDHI, S., WALTERS, R. & LYON, R. 1999. Flammability study of advanced engineering thermoplastics. *Society for the Advancement of Material and Process Engineering, Evolving and Revolutionary Technologies for the New Millenium,* 44, 1142-1150.
GANN, R. G., BABRAUSKAS, V., PEACOCK, R. D. & HALL, J. R. 1994. Fire conditions for smoke toxicity measurement. *Fire and materials,* 18, 193-199.
GOLDBERG, V., KOLESNIKOVA, N., PAVERMAN, N., KAVUN, S., STOTT, P. & GELBIN, M. 2001. Thermo-oxidative degradation of linear low density poly (ethylene) in the presence of carbon black: a kinetic approach. *Polymer degradation and stability,* 74, 371-385.
HAGGERTY, J. S. & CANNON, W. R. 1981. Sinterable powders from laser-driven reactions. *Laser-induced chemical processes.* Springer.

HARTZELL, G. E. & EMMONS, H. W. 1988. The fractional effective dose model for assessment of toxic hazards in fires. *Journal of fire sciences,* 6, 356-362.
HEFFINGTON, W., PARKS, G., SULZMANN, K. & PENNER, S. Studies of methane-oxidation kinetics. Symposium (International) on Combustion, 1977. Elsevier, 997-1011.
HILADO, C. J. 1982. *Flammability Handbook for Plastics,* Westport Technomic.
HUGGETT, C. 1980. Estimation of Rate of Heat Release by Means of Oxygen Consumption Measurements. *Fire and Materials,* 4, 61-65.
HULL, T. R. & KANDOLA, B. K. 2009. *Fire retardancy of polymers: new strategies and mechanisms,* Royal Society of Chemistry.
HULL, T. R., WITKOWSKI, A. & HOLLINGBERY, L. 2011. Fire retardant action of mineral fillers. *Polymer degradation and stability,* 96, 1462-1469.
HURLEY, M. J., GOTTUK, D. T., HALL JR, J. R., HARADA, K., KULIGOWSKI, E. D., PUCHOVSKY, M., WATTS JR, J. M. & WIECZOREK, C. J. 2015. *SFPE handbook of fire protection engineering,* Springer.
INTERNATIONAL, A. 2013. *Standard Test Method for Heat of Combustion of Liquid Hydrocarbon Fuels by Bomb Calorimeter (precision Method),* ASTM International.
JANSSENS, M. Measuring and Predicting Burning rate. *In:* VYTENIS BABRAUSKAS, R. G., STEPHEN GRAYSON, ed. Hazards of Combustion Products, November 2008 The Royal Society, London, UK. Interscience Communications Ltd.
JANSSENS, M. & PARKER, W. J. 1992. Oxygen consumption calorimetry. *Heat Release in Fires,* 3, 31-59.
KASHIWAGI, T. 1979. Experimental observation of radiative ignition mechanisms. *Combustion and Flame,* 34, 231-244.
KENNEDY, I. M. 1997. Models of soot formation and oxidation. *Progress in Energy and Combustion Science,* 23, 95-132.
KISHORE, K. & SANKARALINGAM, S. 1986. Effect of pressure on polymer ignition. *Journal of fire sciences,* 4, 94-99.
KRUGER, H. J., FOCKE, W. W., MHIKE, W., TAUTE, A., ROBERSON, A. & OFOSU, O. 2014. Cone calorimeter study of polyethylene flame retarded with expandable graphite and intumescent fire-retardant additives. *Journal of Fire Sciences,* 32, 498-517.
LE BRAS, M., CAMINO, G., BOURBIGOT, S., DELOBEL, R. 1998. Fire Retardancy of Polymers: The Use of Intumescence. *The Royal Society of Chemistry (Cambridge, UK).*
LINTERIS, G. 2011. Numerical simulations of polymer pyrolysis rate: Effect of property variations. *Fire and Materials,* 35, 463-480.
LU, S.-Y. & HAMERTON, I. 2002. Recent developments in the chemistry of halogen-free flame retardant polymers. *Progress in polymer science,* 27, 1661-1712.
LYON, R. & JANSSENS, M. 2005. Polymer Flammability, DOT/FAA/AR-05/14. *National Technical Information Service, Springfield, VA.*
LYON, R. E. 1998. Pyrolysis kinetics of char forming polymers. *Polymer Degradation and Stability,* 61, 201-210.
LYON, R. E. 2000a. Heat release kinetics. *Fire and Materials,* 24, 179-186.
LYON, R. E. 2000b. *Solid-state thermochemistry of flaming combustion,* Marcel Dekker, Inc., NY.
LYON, R. E. 2002. Fire-Resistant Elastomers.
LYON, R. E. & WALTERS, R. N. 2004. Pyrolysis combustion flow calorimetry. *Journal of Analytical and Applied Pyrolysis,* 71, 27-46.

LYON, R. E., WALTERS, R.N., STOLIAROV, S.I., 2007. Screening Flame Retardants for Plastics using Microscale Combustion Calorimetry. *Society of Plastics Engineers (U.S.)*.
MADRZYKOWSKI, D. & STROUP, D. 2008a. Flammability hazard of materials. *Fire protection handbook,* 1, 31-48.
MADRZYKOWSKI, D. M. & STROUP, D. W. 2008b. Flammability Hazard of Materials. *Fire Protection Handbook 20th Edition,* 1.
MHIKE, W., FERREIRA, I. V., LI, J., STOLIAROV, S. I. & FOCKE, W. W. 2015a. Flame retarding effect of graphite in rotationally molded polyethylene/graphite composites. *Journal of Applied Polymer Science,* 132.
MHIKE, W., FERREIRA, I. V. W., LI, J., STOLIAROV, S. I. & FOCKE, W. W. 2015b. Flame retarding effect of graphite in rotationally molded polyethylene/graphite composites. *Journal of Applied Polymer Science,* 132.
MHIKE, W. & FOCKE, W. W. 2013. Surface resistivity and mechanical properties of rotationally molded polyethylene/graphite composites. *Journal of Vinyl and Additive Technology,* 19, 258-270.
MHIKE, W., FOCKE, W. W. & ASANTE, J. K. 2017. Rotomolded antistatic and flame-retarded graphite nanocomposites. *Journal of Thermoplastic Composite Materials,* 0892705717712634.
MOURITZ, A., MATHYS, Z. & GIBSON, A. 2006. Heat release of polymer composites in fire. *Composites Part A: Applied science and manufacturing,* 37, 1040-1054.
MOURITZA, A. P., MATHYSB, Z, GIBSON, A.G. 2005. Heat release of polymer composites in fire. *Composites: Part A (2006),* 37, 1040–1054.
MULHOLLAND, G., JANSSENS, M., YUSA, S., TWILLEY, W. & BABRAUSKAS, V. 1991. The effect of oxygen concentration on CO and smoke produced by flames. *Fire Safety Science,* 3, 585-594.
MULHOLLAND, G. W. 1995. Smoke production and properties. *SFPE handbook of fire protection engineering,* 3, 2-258.
MWAKIKUNGA, B. W., FORBES, A., SIDERAS-HADDAD, E., ERASMUS, R. M., KATUMBA, G. & MASINA, B. 2008. Synthesis of tungsten oxide nanostructures by laser pyrolysis. *International Journal of Nanoparticles,* 1, 185-202.
NIELSEN, J. B. 2017. *Smouldering* [Online]. Available: https://en.wikipedia.org/wiki/Smouldering [Accessed 28 November 2017 2017].
OHLEMILLER, T. J. 1985. Modeling of smoldering combustion propagation. *Progress in Energy and Combustion Science,* 11, 277-310.
OHLEMILLER, T. J. 1986. *Smoldering combustion,* Center for Fire Research Berkeley.
PAL, G., MACSKASY, H., 1991. *PLASTICS Their Behaviour in Fires,* Budapest, Akademiai Kiado.
PATEL, P., HULL, T. R., STEC, A. A. & LYON, R. E. 2011. Influence of physical properties on polymer flammability in the cone calorimeter. *Polymers for Advanced Technologies,* 22, 1100-1107.
PEACOCK, R. D. & BABRAUSKAS, V. 1991. Analysis of large-scale fire test data. *Fire Safety Journal,* 17, 387-414.
PEARCE, E. 2012. *Flame-retardant polymeric materials,* Springer Science & Business Media.
PETRELLA, R. V. 1994. The Assessment of Full-Scale Fire Hazards from Cone Calorimeter Data. *Journal of Fire Sciences,* 12, 14-43.
PITTS, W. M. 1994. *The global equivalence ratio concept and the prediction of carbon monoxide formation in enclosure fires,* US Department of Commerce, Technology Administration, National Institute of Standards and Technology.

REIN, G. 2009. Smouldering combustion phenomena in science and technology.
RESHETNIKOV, S. M. & RESHETNIKOV, I. S. 1999. Oxidation kinetic of volatile polymer degradation products. *Polymer degradation and stability,* 64, 379-385.
RISTAU, W. T. & VANDERBORGH, N. E. 1971. Laser-induced degradation of hydrocarbon compounds analyzed using gas-liquid chromatography. *Analytical Chemistry,* 43, 702-707.
SACRISTÁN, M., HULL, T. R., STEC, A. A., RONDA, J. C., GALIÀ, M. & CÁDIZ, V. 2010. Cone calorimetry studies of fire retardant soybean-oil-based copolymers containing silicon or boron: Comparison of additive and reactive approaches. *Polymer Degradation and Stability,* 95, 1269-1274.
SCHAEFFER, R. & PEARSON, R. 1969. Reaction of carbon vapor produced by laser evaporation of graphite. *Journal of the American Chemical Society,* 91, 2153-2154.
SCHARTEL, B. & HULL, T. 2007a. Development of fire-retarded materials—Interpretation of cone calorimeter data. *Fire and materials,* 31, 327-354.
SCHARTEL, B. & HULL, T. R. 2007b. Development of fire-retarded materials—Interpretation of cone calorimeter data. *Fire and Materials,* 31, 327-354.
SHAFIZADEH, F. 1984. The chemistry of pyrolysis and combustion. ACS Publications.
SONNIER, R., DOREZ, G., VAHABI, H., LONGUET, C. & FERRY, L. 2014. FTIR-PCFC coupling: A new method for studying the combustion of polymers. *Combustion and Flame,* 161, 1398-1407.
STANDARD, A. 2002. Standard test method for heat of combustion of liquid hydrocarbon fuels by bomb calorimeter. *D240*.
SUSOTT, R. A., SHAFIZADEH, F. & AANERUD, T. W. 1979. Quantitative thermal analysis technique for combustible gas detection. *J Fire Flammability,* 10, 94-104.
TERRILL, J. B., MONTGOMERY, R. R. & REINHARDT, C. F. 1978. Toxic gases from fires. *Science,* 200, 1343-1347.
TEWARSON, A. 1994. Flammability parameters of materials: ignition, combustion, and fire propagation. *Journal of Fire & Flammability,* 12, 329-356.
TEWARSON, A. 2002a. Generation of heat and chemical compounds in fires. *SFPE handbook of fire protection engineering,* 3, 83-161.
TEWARSON, A. 2002b. Generation of Heat and Chemical Compounds in Fires. *SFPE Handbook of Fire Protection Engineering.* 3rd Edition ed. Boston: The National Fire Protection Association Press.
TEWARSON, A. & PION, R. 1976. Flammability of plastics—I. Burning intensity. *Combustion and Flame,* 26, 85-103.
THORNTON, W. M. 1917. The Relation of Oxygen to the Heat of Combution of Organic Compounds. *Philosophical Magazine,* 33, 196-203.
WALTERS, R., GRANVILLE, A. & LYON, R. A microscale heat release rate device. TECHNICAL PAPERS OF THE ANNUAL TECHNICAL CONFERENCE-SOCIETY OF PLASTICS ENGINEERS INCORPORATED, 1996. SOCIETY OF PLASTICS ENGINEERS INC, 2462-2467.
WALTERS, R. N., HACKETT, S. M. & LYON, R. E. 2000. Heats of combustion of high temperature polymers. *Fire and Materials,* 24, 245-252.
WALTERS, R. N. & LYON, R. E. 1997. Microscale combustion calorimeter for determining flammability parameters of materials. *Evolving Technologies for the Competitive Edge.,* 42, 1335-1344.
WALTERS, R. N. & LYON, R. E. 2003. Molar group contributions to polymer flammability. *Journal of Applied Polymer Science,* 87, 548-563.

ZHOU, D.-S., XU, N., LI, L., JI, G. & XUE, G. 2003. Surface reactions on polymer thin films studied by surface-enhanced Raman scattering. *The Journal of Physical Chemistry B,* 107, 2748-2751.

APPENDICES

APPENDIX I: Laser pyrolysis-thermogravimetric energy balance equations

The laser-pyrolysis-TGA based energy-balance equation is:

$$I_0 \Delta A e^{-\sum \alpha_i p_i x}\left[1-e^{-\sum \alpha_i p_i \Delta x}\right] = C_p \frac{m_i}{M_i}\frac{\Delta V}{V} T_{\max}\gamma e^{-\gamma t} + \frac{\Delta H \Delta V}{M_i}\frac{dm_i}{dt} + \varepsilon\sigma A\left[T_{\max}^4\left(1-e^{-\gamma t}\right)^4 - T_s^4\right]$$
$$+ \kappa_{conv}\left(T_{\max}\left(1-e^{-\gamma t}\right)-T_s\right) + 2\pi r_{beam} h K_s\left(T_{\max}-T_{pan}\right) + 2\pi\tau_{pan} h K_{pan}\left(T_{pan}-T\right) \quad \text{(I.1)}$$

The expression that describes how sample mass varies in time and temperature, and laser beam energy can be described from equation (I.1). The Mathematica solution for mass loss comes as follows:

$$m = \sum_{i=1}^{n} m_i$$
$$= \frac{1}{V_0\gamma\Delta H C_p^4}\left(e^{-3\gamma t - \frac{e^{-\gamma C_p t}(T_{\max}-T_s)}{V_0\Delta H}}\left(K_1+K_2+K_3+K_4\left(\gamma V_0\Delta H C_1 + K_{41}\left(\mu P_{laser}+2k_{conv}T+2A\varepsilon\sigma T_s^4\right)\right)+K_5\right)\right) \quad \text{(I.2)}$$

where

$$K_1 = -6AV^4(\Delta H)^4\varepsilon\sigma\exp\left(3t\gamma + \frac{C_p(T-T_s)\exp(-t\gamma)}{V.\Delta H}\right) \quad \text{(I.3)}$$

$$K_2 = 2AV^3(\Delta H)^3\varepsilon\sigma C_p\left(3T+\left(4e^{t\gamma}-3\right)T_s\right)\exp\left(2t\gamma + \frac{C_p(T-T_s)\exp(-t\gamma)}{V.\Delta H}\right) \quad \text{(I.4)}$$

$$K_3 = -AV^2(\Delta H)^2\varepsilon\sigma C_p^2\left(3T^2+2\left(4e^{t\gamma}-3\right)TT_s+\left(3-8e^{t\gamma}+6e^{2t\gamma}\right)T_s^2\right)\exp\left(2t\gamma + \frac{C_p(T-T_s)\exp(-t\gamma)}{V.\Delta H}\right) \quad \text{(I.5)}$$

$$K_4 = C_p^4\exp(3t\gamma) \quad \text{(I.6)}$$

$$K_{41} = ExpIntegralEi\left[\frac{C_p(T-T_s)\exp(-t\gamma)}{V.\Delta H}\right] \quad \text{(I.7)}$$

$$K_5 = -AV(\Delta H)\varepsilon\sigma C_p^3\left[e^{3t\gamma}k_{conv} + A\varepsilon\sigma\left(\begin{array}{l} T^3+2\left(4e^{t\gamma}-3\right)T^2T_s+ \\ \left(3-8e^{t\gamma}+6e^{2t\gamma}\right)TT_s^2+ \\ \left(-1+4e^{t\gamma}-6e^{2t\gamma}+4e^{3t\gamma}\right)T_s^3\end{array}\right)\right]\exp\left(\frac{C_p(T-T_s)\exp(-t\gamma)}{V.\Delta H}\right) \quad \text{(I.8)}$$

APPENDIX II: Combustion gas phase kinetics

Experimental data and kinetic modelling has shown that burning rate is particularly sensitive to chemical reactions which involve certain active free radicals of fuel ($R^{\bullet}$), oxygen ($O^{\bullet}$), hydrogen ($H^{\bullet}$), hydroxyl ($HO^{\bullet}$) and phosphorus or halogen ($X^{\bullet}$) which follow (Lyon and Janssens, 2005)

$RH \xrightarrow{k_1} R^{\bullet} + H^{\bullet}$	Initiation
$H^{\bullet} + O_2 \xrightarrow{k_2} HO^{\bullet} + O^{\bullet}$	Branching
$HO^{\bullet} + CO \xrightarrow{k_3} CO_2 + H^{\bullet}$	Propagation (and primary heat-producing reaction)
$HO^{\bullet} + H_2 \xrightarrow{k_4} H_2O + H^{\bullet}$	Propagation
$H^{\bullet} + O_2 \xrightarrow{k_5} HOO^{\bullet}$	Propagation
$H^{\bullet} + HO^{\bullet} \xrightarrow{k_6} H_2O$	Termination
$H^{\bullet} + HX \xrightarrow{k_7} H_2 + X^{\bullet}$	Inhibition
$HO^{\bullet} + HX \xrightarrow{k_8} H_2O + X^{\bullet}$	Inhibition

Where k_1 to k_8 are rate constants.

APPENDIX III: Energy balance equations for the burning of a polymer

The energy balance equations described in this Section relate to the well-mixed fuel and air situation above a burning polymer slab. This situation is illustrated by Figure 8 in the main text. The energy balance equation for a decomposing slab of polymeric material can be solved from the first law of thermodynamics.

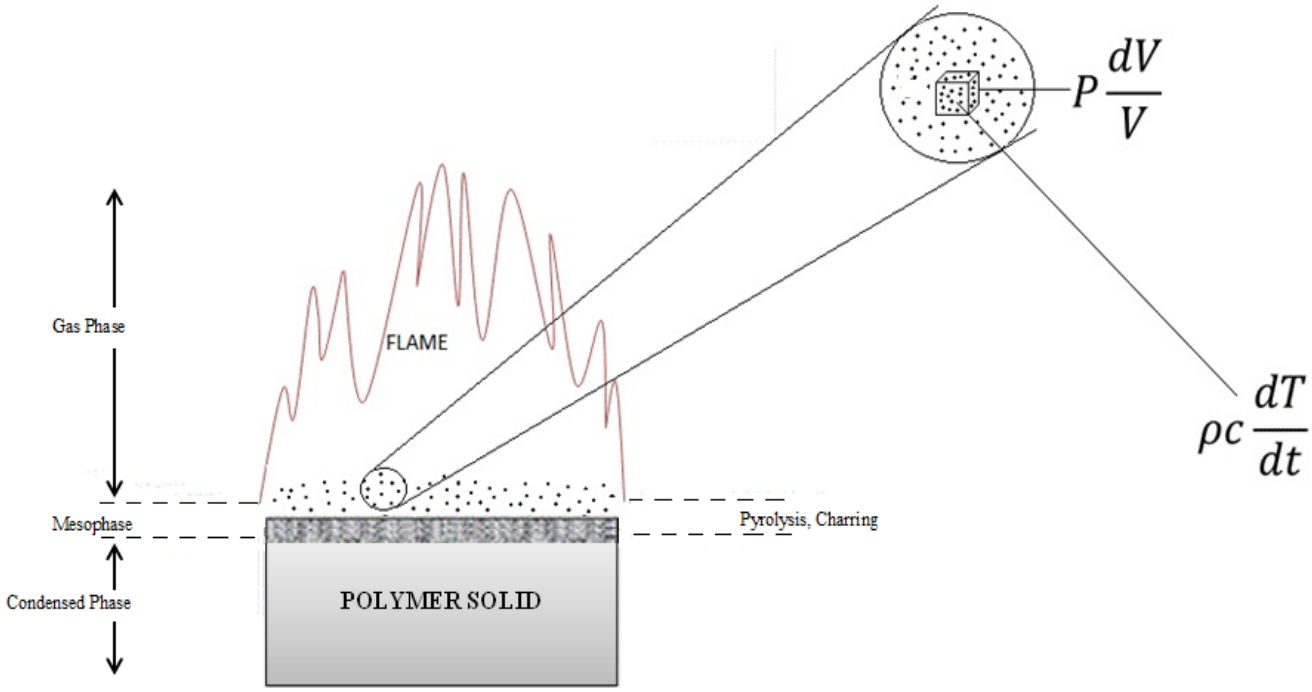

Figure 27: Combustion gas phase energy balance

Gas phase. Starting from the first law of thermodynamics:

$$\boldsymbol{dU + PdV = dQ} \qquad \text{(III.1)}$$

where $\boldsymbol{dU}$ is the internal energy and $\boldsymbol{dQ}$ is the change in heat content, it can be shown that the energy balance for a well-mixed combustion zone is given by (Lyon and Janssens, 2005)

$$\boldsymbol{\rho c\frac{\partial T}{\partial t} + P\frac{dV}{dt} = \dot{Q} - convection - radiation} \qquad \text{(III.2)}$$

which can be written as follows,

$$\boldsymbol{\rho c\frac{\partial T}{\partial t} + P\frac{dV}{dt} = \dot{Q} - hS(T - T_a) - \varepsilon\sigma S\left(T^4 - T_a^4\right)} \qquad \text{(III.3)}$$

where $\boldsymbol{\rho}$ is the instantaneous density, $\boldsymbol{c}$ the heat capacity, volume $\boldsymbol{V}$and temperature $\boldsymbol{T}$ of fuel-air and combustion products mixture, the average heat transfer coefficient $\boldsymbol{\bar{h}}$ at the boundary between the combustibles and the environment with surface area $\boldsymbol{S}$ of temperature $\boldsymbol{T}$ and pressure $\boldsymbol{P}$. The fuel-air mixture reacts generating the power density $\boldsymbol{\dot{Q} = \widetilde{Q}^V}$ (heat of combustion per unit volume) (Lyon and Janssens, 2005).

Figure 27 illustrates the energy balance equation (III.3) in the gas phase for the well mixed fuel-air mixture which reacts generating the power density $\dot{\boldsymbol{Q}} = \widetilde{\boldsymbol{Q}}^{\boldsymbol{V}}$, where one part is accumulated in the reaction volume as a result of temperature rise in fuel air mixture. The second part is lost to the surrounding at room temperature $\boldsymbol{T_a}$ by convection and radiation.

Char yield. The initial stages of a burning material can produce primary pyrolysis volatiles and char residues. The first-order thermal decomposition process that results to the products of combustion has been presented (Hull et al., 2011, Mhike et al., 2015a, Patel et al., 2011). The char yield of the pyrolysed material is equal to the fraction of residue mass. This is a result of an anaerobic pyrolysis which represents the char temperature in a fire. Hence, the fuel generation rate in a fire under anaerobic pyrolysis is

$$-\boldsymbol{dm'} = \boldsymbol{k_p m' e^{-\frac{E_a}{RT}} dt} \qquad \text{(III.4)}$$

Where char yield can be determined experimentally from the mass fraction of the residue remaining. Integrating (III.2) we have,

$$\int_0^{\tau} \frac{\boldsymbol{dm'}}{\boldsymbol{m'}} = -\boldsymbol{A k_p} \int \boldsymbol{e^{-\frac{E_a}{RT}} dt} \qquad \text{(III.5)}$$

Such that,

$$\boldsymbol{ln}\left[\frac{\boldsymbol{m'(\tau)}}{\boldsymbol{m'(0}}\right] = -\boldsymbol{A k_p} \int \boldsymbol{e^{-\frac{E_a}{RT}} dt} \qquad \text{(III.6)}$$

where $\boldsymbol{m'}$ is the volatile fuel mass, the constant of mass loss rate $\boldsymbol{k_p}$ in terms of frequency factor $\boldsymbol{A}$ and $\boldsymbol{E_a}$ the activation energy. Hence, equation (IV.3) describes the non-isothermal fuel generation rate at an arbitrary temperature $\boldsymbol{T(t)}$ in the mesophase (Lyon and Janssens, 2005). The main pyrolysis products can be represented by a scheme of first order thermal degradation processes which sufficiently represent the kinetics of fuel generation in the mesophase given as (Lyon and Janssens, 2005)

Mesophase. A series of processes define the thermal degradation of a polymer at rate constant k_d leading to a reactive intermediate state I^*. At this state the gas (G) is produced with rate constant k_g and/or the char (C) with k_c.

Polymer $\xrightarrow{k_d}$ Intermediate(I^*)

$I^* \xrightarrow{k_g}$ Gas (G)

$I^* \xrightarrow{k_c}$ Char (C)

The rate constants $\boldsymbol{k_c}$(char) and $\boldsymbol{k_g}$(gas) can be represented in the Arrhenius form with common activation energy:

$$\boldsymbol{k_c = A_c e^{-\frac{E_a}{RT}}} \quad \text{and} \quad \boldsymbol{k_g = A_g e^{-\frac{E_g}{RT}}} \tag{III.7}$$

This kinetic analysis yields the following expression for the equilibrium char fraction (Lyon and Janssens, 2005) is

$$\mathbf{Y_c}(\boldsymbol{T}) = \left(\mathbf{1} + \frac{\boldsymbol{A_g}}{\boldsymbol{A_c}} \boldsymbol{e}^{-\frac{\boldsymbol{E_g - E_c}}{\boldsymbol{RT}}}\right)^{\mathbf{-1}} \tag{III.8}$$

which is expressed in terms of constant rates of mass loss ($\boldsymbol{k_c}$, $\boldsymbol{k_g}$) as defined by the frequency factors ($\boldsymbol{A_g}, \boldsymbol{A_c}$) and activation energies ($\boldsymbol{E_g}$,$\boldsymbol{E_c}$) for the gas and char formation. The equilibrium char fraction represents group contribution for charring polymers (Linteris, 2011).

Condensed phase. The ignition time and burning rate of a polymer are consequences of heat transport and storage. The thermophysical properties at room temperature have been gathered for a number of plastic materials (Hull et al., 2011). Thermal inertia is the product of three properties, that is, thermal conductivity, density and heat capacity. Thermal inertia is a directive of material surface temperature to reach ignition temperature. The lower values of thermal inertia lead to higher surface temperatures resulting from the applied heat flux. The values of thermal inertia for some material can be found in the literature (DiGuiseppi et al., 1998). However, thermal inertia can be affected by the way the properties are measured. The temperature dependence of thermal inertia properties for an amorphous polymer can be estimated by using the following approximations:

$$\boldsymbol{\kappa(T) = \kappa_0 \sqrt{T/T_o}} \tag{III.9}$$

$$\boldsymbol{\rho(T) = \rho_0 \sqrt{T_o/T}} \tag{III.10}$$

$$\boldsymbol{c(T) = c_0 (T/T_o)} \tag{III.11}$$

Therefore, the approximate temperature dependence can be expressed as follow

$$\boldsymbol{\kappa(T)\rho(T)c(T) \approx \kappa_0 \rho_0 c_0 \frac{T}{T_0} = (\kappa \rho c)_0 \frac{T}{T_0}} \tag{III.12}$$

and $\boldsymbol{\kappa_0}$, $\boldsymbol{\rho_0}$, $\boldsymbol{c_0}$ are known values at room temperature $\boldsymbol{T_0}$ (Lyon and Janssens, 2005). Thermal diffusivity $\boldsymbol{\alpha = \kappa/\rho c}$ is a quantity relevant to unsteady heat transfer analysis, such that

$$\boldsymbol{\alpha = \frac{\kappa(T)}{\rho(T)c(T)} = \alpha_0} \tag{III.13}$$

APPENDIX IV. Laser pyrolysis-thermogravimetric analysis results

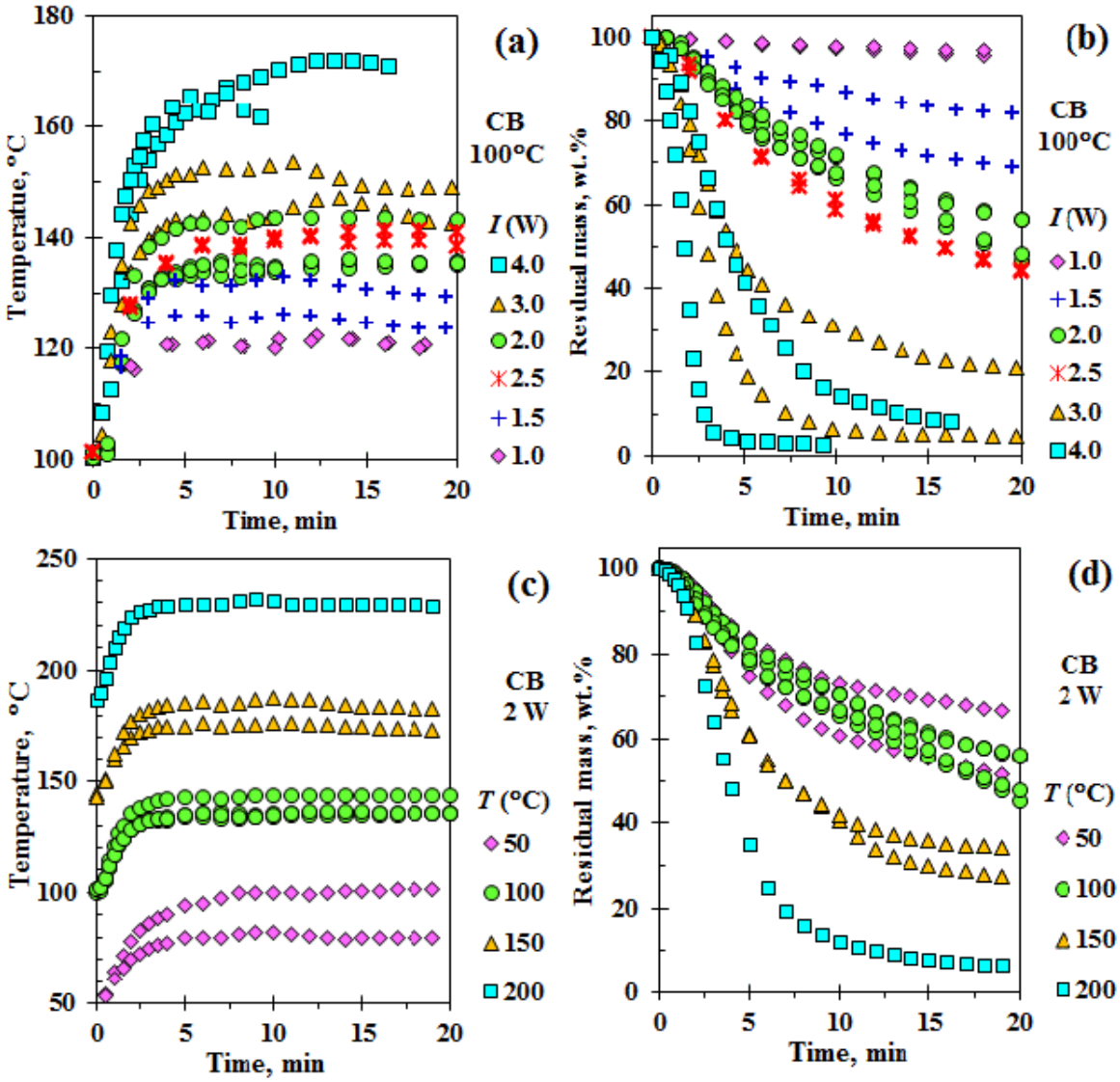

Figure 28: Carbon black (CB) composites LPy-TGA (a) sample temperature changes from 100°C TGA isothermal temperature at varied laser beam energy (b) mass loss at 100°C TGA isothermal temperature with varied laser beam energy (c) sample temperature changes at 2 Watt laser beam energy with varied TGA isothermal temperatures (d) mass loss at 2 W laser beam energy with varied TGA isothermal temperatures.

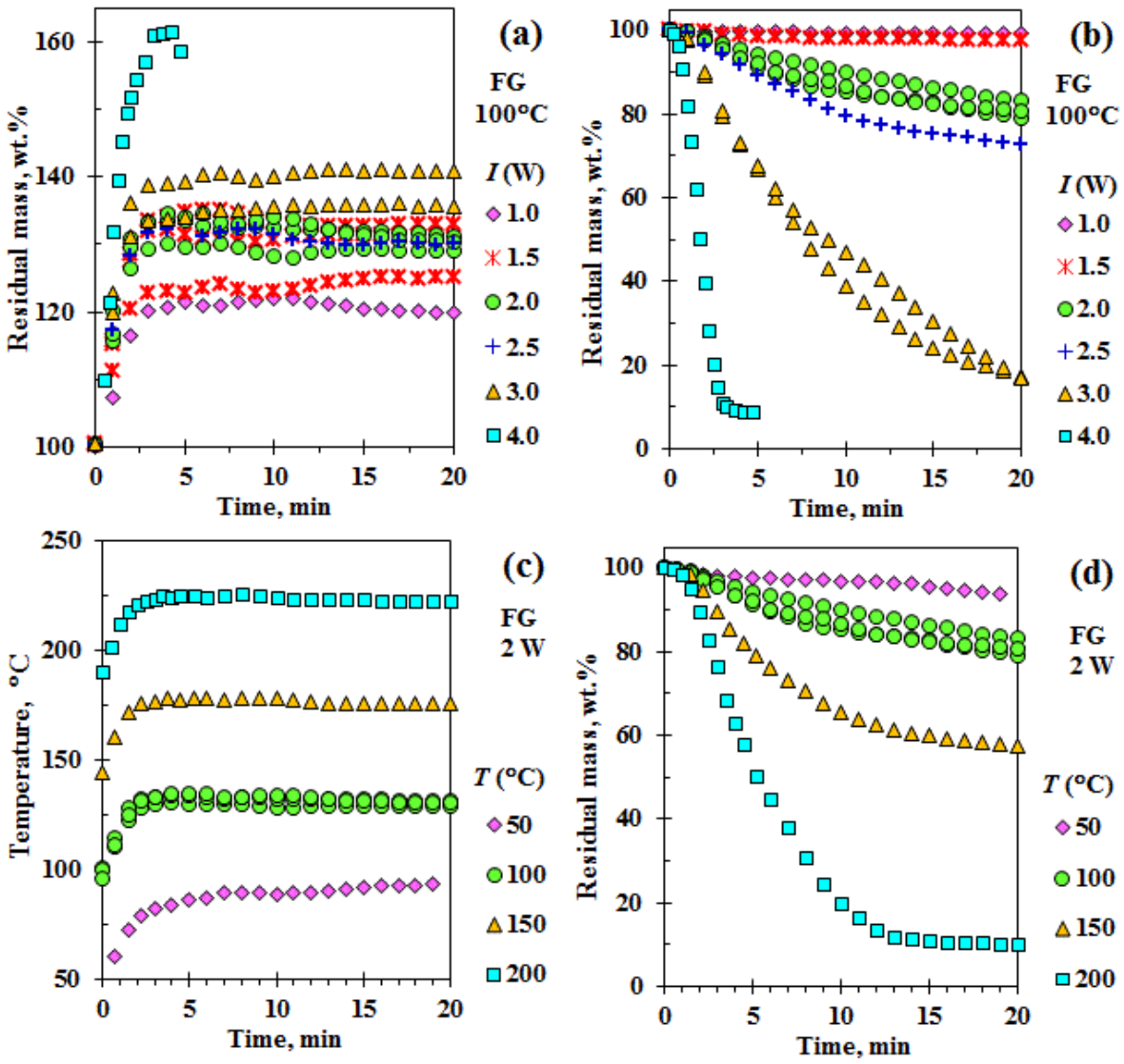

Figure 29: Flake graphite (FG) composites LPy-TGA (a) sample temperature changes from 100°C TGA isothermal temperature at varied laser beam energy (b) mass loss at 100°C TGA isothermal temperature with varied laser beam energy (c) sample temperature changes at 2 Watt laser beam energy with varied TGA isothermal temperatures (d) mass loss at 2 W laser beam energy with varied TGA isothermal temperatures.

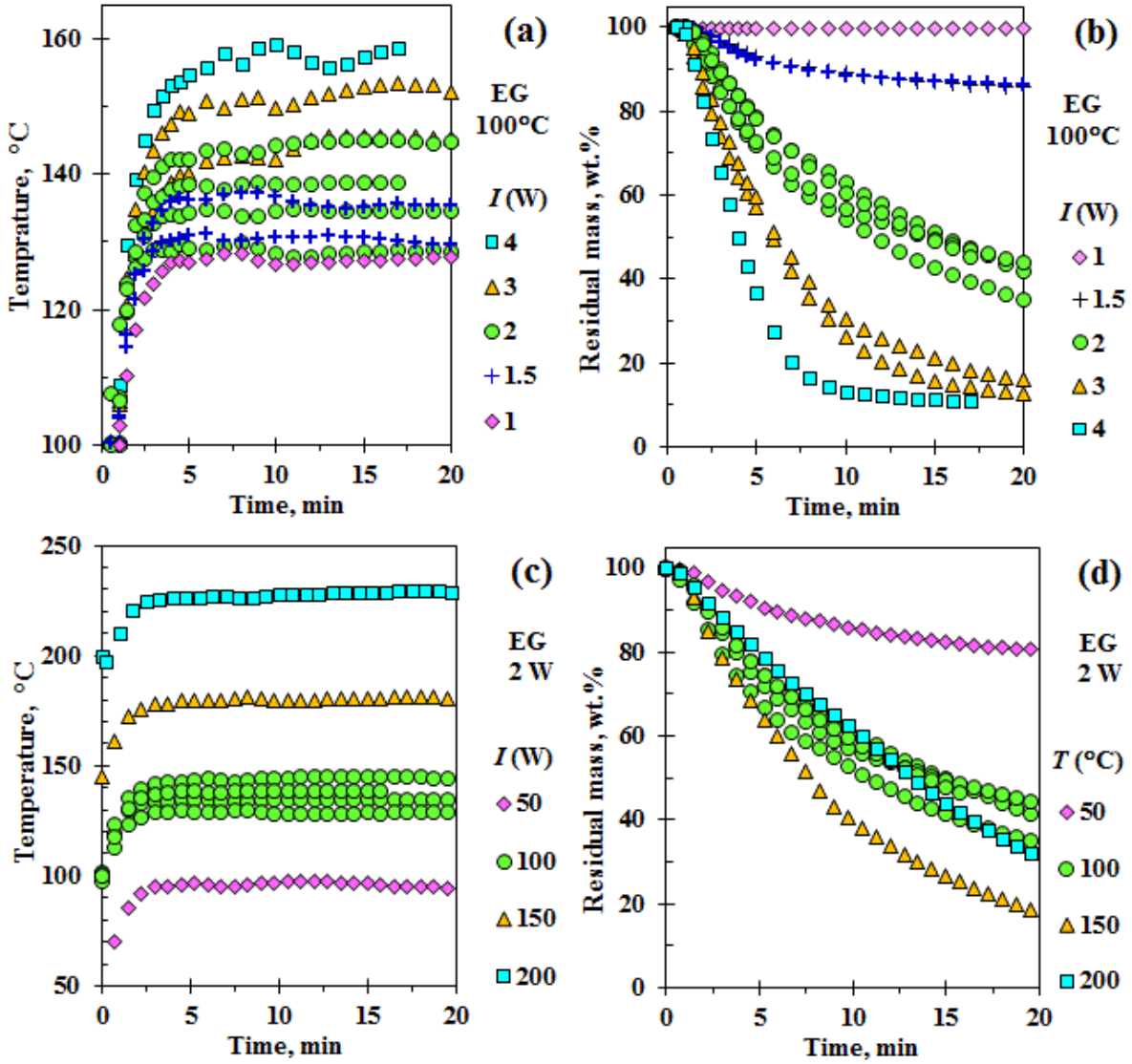

Figure 30: Expandable graphite (EG) composites LPy-TGA (a) sample temperature changes from 100°C TGA isothermal temperature at varied laser beam energy (b) mass loss at 100°C TGA isothermal temperature with varied laser beam energy (c) sample temperature changes at 2 Watt laser beam energy with varied TGA isothermal temperatures (d) mass loss at 2 W laser beam energy with varied TGA isothermal temperatures.

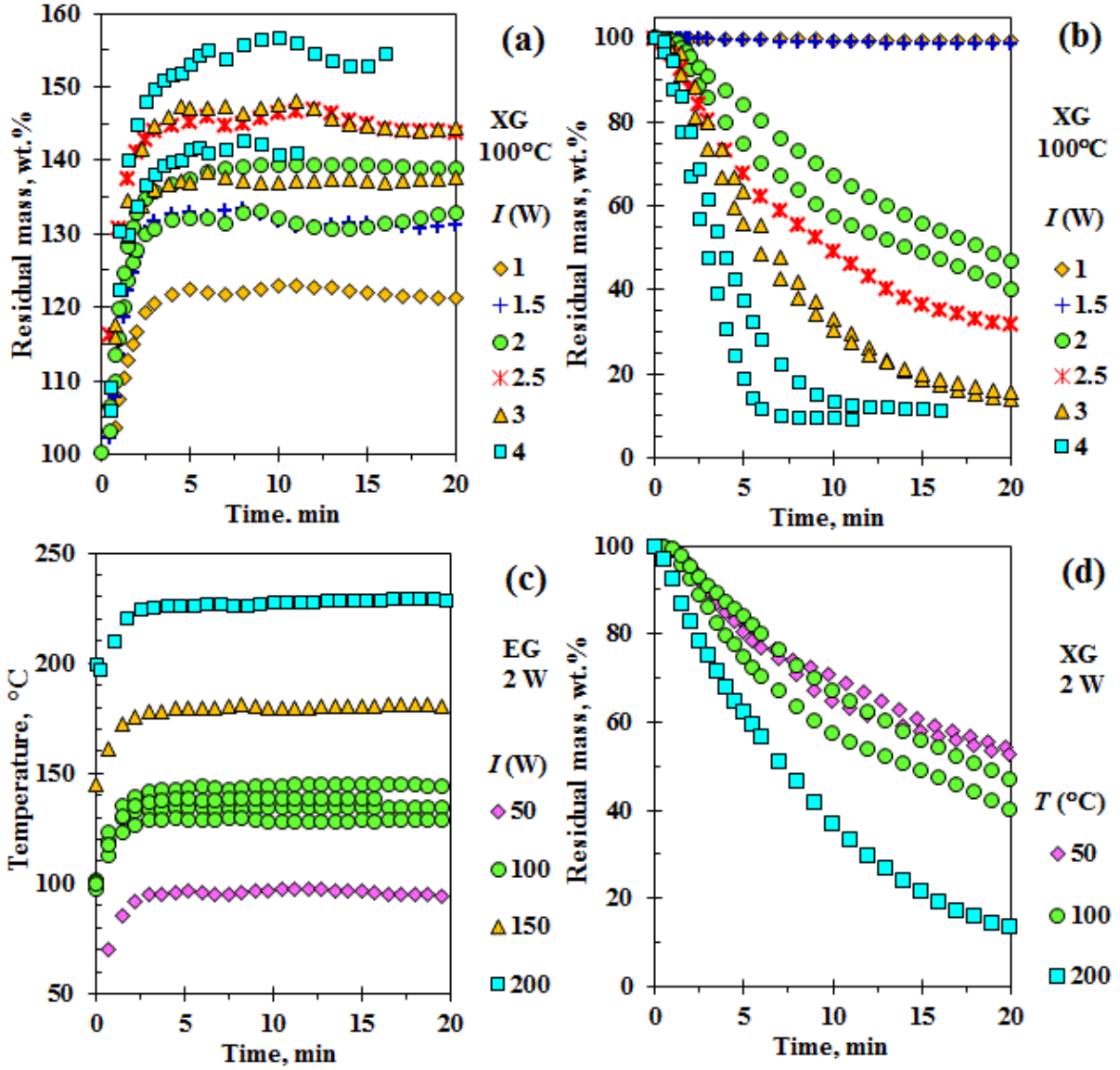

Figure 31: Exfoliated graphite (XG) composites LPy-TGA (a) sample temperature changes from 100°C TGA isothermal temperature at varied laser beam energy (b) mass loss at 100°C TGA isothermal temperature with varied laser beam energy (c) sample temperature changes at 2 Watt laser beam energy with varied TGA isothermal temperatures (d) mass loss at 2 W laser beam energy with varied TGA isothermal temperatures.